Optimal Selection of Basis Functions for Minimum-Effort Tracking Control of Nonminimum Phase Systems Using Filtered Basis Functions

Keval S. Ramani
Smart and Sustainable Automation Research Lab
Department of Mechanical Engineering
University of Michigan,
2350 Hayward, Ann Arbor, MI, 48109
e-mail: ksramani@umich.edu
Student Member

Molong Duan
Smart and Sustainable Automation Research Lab
Department of Mechanical Engineering
University of Michigan,
2350 Hayward, Ann Arbor, MI, 48109
e-mail: molong@umich.edu
Student Member

Chinedum E. Okwudire
Smart and Sustainable Automation Research Lab
Department of Mechanical Engineering
University of Michigan,
2350 Hayward, Ann Arbor, MI, 48109
e-mail: okwudire@umich.edu (Corresponding Author)
Member ASME

A. Galip Ulsoy
Department of Mechanical Engineering
University of Michigan,
2350 Hayward, Ann Arbor, MI, 48109
e-mail: ulsoy@umich.edu
ASME Fellow

ABSTRACT

Accurate tracking of nonminimum phase (NMP) systems is well known to require large amounts of control effort. It is, therefore, of practical value to minimize the effort

needed to achieve a desired level of tracking accuracy for NMP systems. There is growing interest in the use of the filtered basis functions (FBF) approach for tracking control of linear NMP systems because of distinct performance advantages it has over other methods. The FBF approach expresses the control input as a linear combination of user-defined basis functions. The basis functions are forward filtered through the dynamics of the plant and the coefficients are selected such that the tracking error is minimized. There is a wide variety of basis functions that can be used with the FBF approach, but there has been no work to date on how to select the best set of basis functions. Towards selecting the best basis functions, the Frobenius norm of the lifted system representation of dynamics is proposed as an excellent metric for evaluating the performance of linear time varying discrete-time tracking controllers, like FBF, independent of the desired trajectory to be tracked. Using the metric, an optimal set of basis functions that minimize the control effort without sacrificing tracking accuracy is proposed. The optimal set of basis functions is shown in simulations and experiments to significantly reduce control effort while maintaining or improving tracking accuracy compared to popular basis functions, like B-splines.

1. INTRODUCTION

Tracking control is a fundamental problem encountered in a wide range of application areas such as manufacturing, robotics and aeronautics. The objective of tracking control is to force the output of the controlled system to follow a desired trajectory as closely as possible. It is also important that this objective is achieved with minimal control effort, e.g., due to power limits of actuators. Excellent tracking accuracy can be achieved using feedforward control by direct inversion of a sufficiently accurate model of

a system (i.e., pole-zero cancellation) [1]. However, when applied to systems with nonminimum phase (NMP) zeros, direct model inversion gives rise to unstable or extremely high control inputs which are unacceptable [1]. There have been several feedforward tracking control methods reported in the literature that are applicable to linear systems with NMP zeros. These methods include NMP zero ignore (NPZ-ignore), zero phase error tracking control (ZPETC) [1], zero magnitude error tracking control (ZMETC), extended bandwidth ZPETC [2], truncated series (TS) [3], direct inversion with bounded reference trajectories [4–8], approximate frequency domain inversion [9], H_∞ matching [10,11], B-spline-based tracking with preview using iterative learning control [12], spline filtering with feedback [13,14], etc. A major shortcoming of most of these methods is that they are not versatile in terms of the systems and/or the desired trajectories to which they are applicable (e.g., several of the methods cannot be applied to nonhyperbolic systems, i.e., systems with zeros on the unit circle) – see [15] for a more detailed discussion of this matter. Moreover, their tracking accuracy varies significantly depending on NMP zero location (in the complex plane) [15].

The filtered basis functions (FBF) approach has recently been gaining interest as an approach for tracking linear systems with NMP zeros [15–19]. The origin of the FBF approach can be traced back to the work of Frueh and Phan [20] on inverse linear quadratic learning in iterative learning control (ILC). It expresses the control input as a linear combination of user-defined basis functions with unknown coefficients. The basis functions are forward filtered using the system dynamics, and their coefficients selected such that tracking error is minimized. Unlike most of the methods discussed above, the FBF method is effective in tracking any desired trajectory, irrespective of the location of

NMP zeros in the *z*-plane (including nonhyperbolic systems [15,17,19]). Moreover, it has been observed by the authors that the FBF method maintains consistent tracking accuracy compared to popular linear time invariant (LTI) discrete-time tracking controllers irrespective of the location of the NMP zero in the *z*-plane [15,17,21].

There is a wide range of basis function available for use with the FBF approach. The choice of basis functions is entirely up to the control engineer. Prior work in the literature has explored cosine signals [20,22], reference trajectory based basis functions [23,24], B-splines [12,17,21], Gaussian radial basis functions [18], etc. However, there has been no study on the optimal selection of basis functions to achieve a desired control objective using the FBF approach. This paper (and, in part, its preliminary version [25]) addresses the problem of optimal basis function selection by making the following original contributions to the literature:

1. It proposes the Frobenius norm of the lifted system representation (LSR) of dynamics as an excellent and appropriate metric for analyzing the performance of LTI and linear time varying (LTV) tracking controllers, independent of desired trajectory. The proposed metric is applicable to any discrete-time linear controller.
2. It demonstrates, using the metric that the tracking accuracy of the FBF approach is solely dependent on the number of basis functions used; it is independent of the type of basis functions and the plant dynamics (e.g., zero location), thus explaining the consistent tracking performance of the FBF approach relative to other tracking controllers.
3. It demonstrates that the metric for FBF's control effort dynamics is dependent on the system dynamics and the type of basis functions used. A methodology for determining

the optimal set of basis functions for achieving a desired level of tracking accuracy with minimum control effort is derived analytically. These optimal basis functions are shown to be singular vectors of the lifted system representation of the plant dynamics.

Section 2 provides some background and motivation for the paper, and Sec. 3 presents the proposed metric, analyzes the FBF method using the metric and derives a methodology for determining the optimal set of basis functions. The discussion in Sec. 3 is validated in Sec. 4, using simulations and experiments. This is followed by conclusions and future work in Sec. 5.

2. BACKGROUND AND MOTIVATION

2.1. Feedforward Tracking Control Problem

Given a discrete-time LTI single input single output (SISO) plant $G(q)$, as shown in Fig. 1, which may represent an open loop or a closed loop controlled system, we can write

$$y(k) = G(q)u(k) \tag{1}$$

where k is the time index, q is the forward shift operator, y and u are the output and control input, respectively. The objective of feedforward tracking control is to design a controller $C(q)$ or find a control input $u(k)$ given by

$$u(k) = C(q)y_d(k) \tag{2}$$

where $y_d(k)$ is the desired trajectory, such that the tracking error, $e(k)$, given by

$$\begin{aligned} e(k) &= y_d(k) - y(k) \\ &= (1 - \underbrace{G(q)C(q)}_{L(q)})y_d(k) = E_{ff}(q)y_d(k) \end{aligned} \tag{3}$$

is minimized. Note that $L(q)$ and $E_{ff}(q)$ are the overall and error dynamics of the controlled system, respectively.

For finite time, $0 \le k \le M$ (where M+1 is the number of discrete points in the trajectory), the desired trajectory, control input, tracking error and output trajectory can be expressed using vectors as

$$\begin{aligned} &\mathbf{y}_d = \begin{bmatrix} y_d(0) & y_d(1) & \dots & y_d(M) \end{bmatrix}^{\mathrm{T}}, \ \mathbf{u} = \begin{bmatrix} u(0) & u(1) & \dots & u(M) \end{bmatrix}^{\mathrm{T}}, \\ &\mathbf{e} = \begin{bmatrix} e(0) & e(1) & \dots & e(M) \end{bmatrix}^{\mathrm{T}}, \ \mathbf{y} = \begin{bmatrix} y(0) & y(1) & \dots & y(M) \end{bmatrix}^{\mathrm{T}} \end{aligned} \tag{4}$$

Accordingly, Eqs. (1), (2) and (3) can be expressed as

$$\mathbf{y} = \mathbf{G}\mathbf{u}; \ \ \mathbf{u} = \mathbf{C}\mathbf{y}_d; \ \ \mathbf{e} = \underbrace{(\mathbf{I} - \mathbf{L})}_{\mathbf{E}_{ff}} \mathbf{y}_d \tag{5}$$

where **G**, **C, L** and $\mathbf{E}_{ff}$ are the lifted system representations (LSRs) of G, C, L and E_{ff}, respectively (see Appendix A for details on LSR), and **I** is the identity matrix of appropriate size.

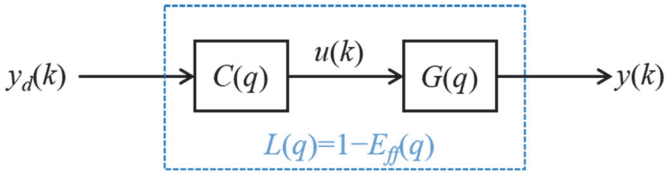

Fig. 1: Block diagram for feedforward tracking control

2.2. Filtered Basis Functions (FBF) Approach

The FBF approach relies on two assumptions:

1. the desired trajectory is known *a priori*; and
2. the control input $u(k)$ is expressed as a linear combination of n+1 user-defined basis functions $\varphi_i(k)$; i.e.,

$$u(k) = \sum_{i=0}^{n} \gamma_i \varphi_i(k) \tag{6}$$

where γ_i are unknown coefficients. Using vectors, Eq. (6) can be expressed as

$$\begin{gathered}\mathbf{u}=\boldsymbol{\Phi}\boldsymbol{\gamma};\\ \boldsymbol{\Phi}=\begin{bmatrix}\boldsymbol{\varphi}_0 & \boldsymbol{\varphi}_1 & \dots & \boldsymbol{\varphi}_n\end{bmatrix},\ \boldsymbol{\varphi}_i=\begin{bmatrix}\varphi_i(0) & \varphi_i(1) & \dots & \varphi_i(M)\end{bmatrix}^{\mathrm{T}},\ \boldsymbol{\gamma}=\begin{bmatrix}\gamma_0 & \gamma_1 & \dots & \gamma_n\end{bmatrix}^{\mathrm{T}}\end{gathered} \tag{7}$$

Hence, for a linear system $G(q)$ (with LSR $\mathbf{G}$), $\mathbf{y}$ can be expressed as

$$\begin{gathered}\mathbf{y}=\tilde{\boldsymbol{\Phi}}\boldsymbol{\gamma};\\ \tilde{\boldsymbol{\Phi}}=\mathbf{G}\boldsymbol{\Phi};\ \ \tilde{\boldsymbol{\varphi}}_i=\mathbf{G}\boldsymbol{\varphi}_i;\ \tilde{\boldsymbol{\Phi}}=\begin{bmatrix}\tilde{\boldsymbol{\varphi}}_0 & \tilde{\boldsymbol{\varphi}}_1 & \dots & \tilde{\boldsymbol{\varphi}}_n\end{bmatrix}\end{gathered} \tag{8}$$

where $\tilde{\boldsymbol{\Phi}}$ represents the filtered basis functions. The control objective is to find the optimal coefficient vector $\boldsymbol{\gamma}$ such that the squared 2-norm of the tracking error, i.e.,

$$\mathbf{e}^{\mathrm{T}}\mathbf{e}=\left(\mathbf{y}_d-\tilde{\boldsymbol{\Phi}}\boldsymbol{\gamma}\right)^{\mathrm{T}}\left(\mathbf{y}_d-\tilde{\boldsymbol{\Phi}}\boldsymbol{\gamma}\right) \tag{9}$$

is minimized; the optimal solution is given by the classical least-squares solution,

$$\boldsymbol{\gamma}^{*}=\left(\tilde{\boldsymbol{\Phi}}^{\mathrm{T}}\tilde{\boldsymbol{\Phi}}\right)^{-1}\tilde{\boldsymbol{\Phi}}^{\mathrm{T}}\mathbf{y}_d \tag{10}$$

Based on Eqs. (5), (7), (8) and (10), the controller dynamics ($C(q)$) and error dynamics ($E_{ff}(q)$) for the FBF controller can be expressed in LSR as

$$\begin{aligned}\mathbf{C}_{FBF}&=\boldsymbol{\Phi}\left(\tilde{\boldsymbol{\Phi}}^{\mathrm{T}}\tilde{\boldsymbol{\Phi}}\right)^{-1}\tilde{\boldsymbol{\Phi}}^{\mathrm{T}}\\ \mathbf{E}_{ff,FBF}&=\mathbf{I}-\underbrace{\tilde{\boldsymbol{\Phi}}\left(\tilde{\boldsymbol{\Phi}}^{\mathrm{T}}\tilde{\boldsymbol{\Phi}}\right)^{-1}\tilde{\boldsymbol{\Phi}}^{\mathrm{T}}}_{\mathbf{L}_{FBF}}\end{aligned} \tag{11}$$

Remark 1: $\mathbf{C}_{FBF}$ and $\mathbf{E}_{ff,FBF}$ both depend on the LSR of the plant, $\mathbf{G}$, as well as the selected basis functions. Both matrices are, in general, non-Toeplitz and non-triangular implying that the FBF controller is, in general, LTV and non-causal [15].

Remark 2: Although, for simplicity, this paper describes the FBF approach in the context of LTI SISO systems, it is applicable to other types of linear systems such as LTV, linear parameter varying (LPV) [18] and multi-input multi-output (MIMO) systems. Reference [17] relaxes the assumption on *a priori* knowledge of the entire desired trajectory using the

local property of B-splines as basis functions. Without loss of generality, this paper assumes that the initial conditions are zero. The authors' prior work [15,17] can be consulted for approaches to incorporate effects of initial conditions into the FBF approach.

2.3. Motivational Case Study

This section motivates the rest of the paper using time-domain simulations based on a simple first order plant

$$G(q) = \frac{q-a}{q-p} \tag{12}$$

where a (a real number) ϵ [−5, 5] and p = 0.5 are the zero and pole of the system, respectively. Note that this first order system has also been used for analysis of simple approximate inversion techniques by Butterworth et al. [26]. In this section, the tracking performance of FBF is analyzed for different basis functions.

For simulations, the desired trajectory (y_d) is a zero-mean white noise signal, with variance equal to 1, M = 1000 and sampling frequency 10 kHz. As discussed in Sec. 1, there is a wide range of basis functions available for use with the FBF method. Here, three types of basis functions are used: (i) discrete cosine transform (DCT) [22], (ii) block pulse functions (BPF) [27] and (iii) B-splines [28]; their expressions are provided in Appendix B. The DCT and BPF basis functions are rudimentary basis functions in frequency-domain and time-domain, respectively, whereas, B-splines are commonly used to parameterize commands sent to manufacturing machines and robots [29].

Figure 2 (a) compares the normalized root mean square (RMS) tracking error $\mathbf{e}_{RMS}/\mathbf{y}_{d,RMS}$ for the three basis functions (n = 990) for various values of a. It must be pointed out that approximate inversion is not generally used for tracking control in the minimum phase (MP) region because $C = G^{-1}$ can be employed (provided a is not poorly damped

[1]). However, the MP region is included in this paper for sake of completeness. The FBF approach demonstrates consistent tracking accuracy, as compared to popular methods in the literature (see Fig. 12 in Appendix C for a comparison with two such popular methods, viz. ZPETC and TS), irrespective of zero location and type of basis functions [15,17,21]. Similar observations have been made in prior work [15,17] and contrasted with other tracking controllers whose tracking accuracy typically varies significantly depending on NMP zero location [3,26]. A theoretical justification for this observation was preliminarily explored in [25], and is further discussed in Sec. 3 below.

Figure 2 (b) compares the normalized RMS control effort of the various basis functions applied to the FBF approach. Notice that there is significant variation in control effort for various basis functions, even when tracking accuracy is similar. For instance, at $a = 1.02$, all the basis functions achieve similar levels of tracking accuracy, but the control effort required by DCT is 370 times that of BPF, whereas, the control effort required by B-splines is 11800 times that required by DCT. In contrast, all the basis functions have very similar values of $\mathbf{e}_{RMS}$ and $\mathbf{u}_{RMS}$ for $-1 \leq a \leq 1$. This suggests that the system dynamics and choice of basis functions play a significant role in the control effort required to achieve a desired level of tracking accuracy using the FBF approach. Hence, a methodology for determining the best set of basis functions for a given plant and desired level of tracking accuracy is needed.

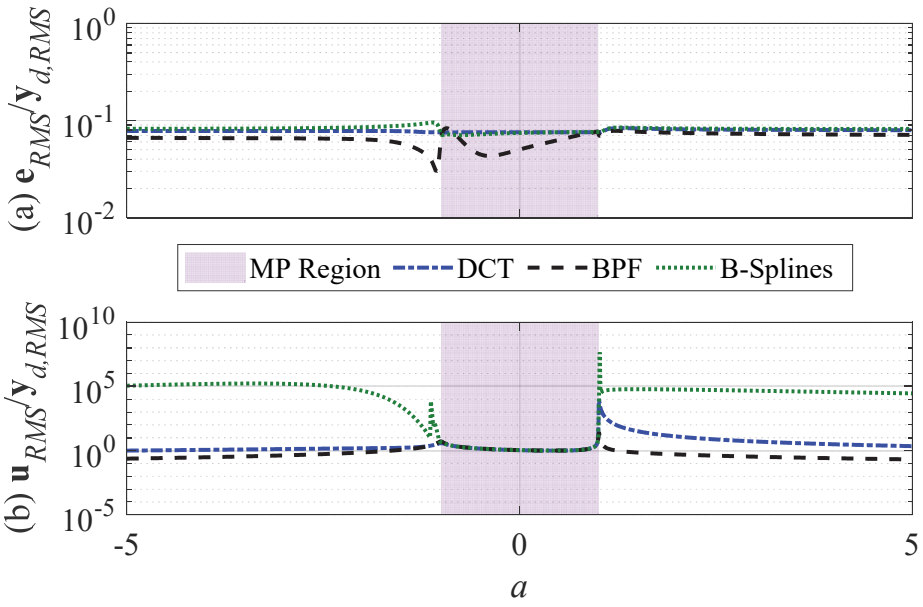

Fig. 2: Effect of basis functions (DCT, BPF and B-splines) on: (a) normalized RMS tracking error and (b) normalized RMS control input for various values of a (M = 1000, n = 990). The methods are also simulated for MP region (shaded) but the system can also be inverted in this region.

3. OPTIMAL SELECTION OF BASIS FUNCTIONS

A suitable metric is needed in order to probe deeper into the observations made in Sec. 2.3 above and provide a methodology for selecting an optimal set of basis functions. While Bode diagrams [3] and magnitude at Nyquist frequency [26] have been used as metrics to analyze LTI tracking controllers, they are not applicable to LTV controller like FBF. In this section, we propose a metric that is suitable for analyzing LTV controllers like FBF, independent of trajectory to be tracked, and utilize the metric to develop a methodology for optimal selection of basis functions for minimum control effort.

3.1. Proposed Metric

For evaluating the tracking accuracy of discrete-time linear controllers (LTI or LTV), we propose the following metric, J_e, based on the Frobenius norm of $\mathbf{E}_{ff}$

$$J_e = \frac{\left\|\mathbf{E}_{ff}\right\|_F}{\sqrt{M+1}}; \qquad \left\|\mathbf{E}_{ff}\right\|_F = \sqrt{trace(\mathbf{E}_{ff}^{\mathrm{T}}\mathbf{E}_{ff})} = \sqrt{\sum_{\forall i}\left\{\sigma_i(\mathbf{E}_{ff})\right\}^2} \tag{13}$$

The Frobenius norm is selected because it considers all singular values/gains (σ_i) of $\mathbf{E}_{ff}$, as opposed to $||\mathbf{E}_{ff}||_2$ (sometimes used in ILC for stability analysis [30]), which considers only the maximum singular value/gain. The square root of (M+1) is included in the metric to ensure that it is uniformly bounded as the length of the trajectory (and size of $\mathbf{E}_{ff}$) grows. Moreover, as shown in Appendix D, for an LTI system,

$$J_e = \frac{\left\|\mathbf{E}_{ff}\right\|_F}{\sqrt{M+1}} \rightarrow \left\|E_{ff}(q)\right\|_2 \quad \text{as} \quad M \rightarrow \infty \tag{14}$$

In other words, J_e approaches the error 2-norm criterion (sometimes used in the design and analysis of tracking controllers [3]). The singular values of $\mathbf{E}_{ff}$ approximate the magnitude of the frequency response of $E_{ff}(q)$ [31]; and $||E_{ff}(q)||_\infty$ is the maximum gain of the system $E_{ff}(q)$ which is approximated by $||\mathbf{E}_{ff}||_2$ (because the 2-norm of a matrix is its maximum singular value) and this approximation is more accurate as $M \rightarrow \infty$.

Note that for a normalized desired trajectory (i.e., $||\mathbf{y}_d||_2 = 1$),

$$\mathbf{e}_{RMS} = \frac{\left\|\mathbf{e}\right\|_2}{\sqrt{M+1}} \leq \frac{\left\|\mathbf{E}_{ff}\right\|_F}{\sqrt{M+1}} = J_e \tag{15}$$

The implication is that J_e is an upper bound on the RMS tracking error ($\mathbf{e}_{RMS}$).

Similarly, control effort requirements can be analyzed using metric, J_c, defined as follows

$$J_c = \frac{\|\mathbf{C}\|_F}{\sqrt{M+1}} \tag{16}$$

and analogously, J_c bounds the RMS control input ($\mathbf{u}_{RMS}$) for a tracking controller with $||\mathbf{y}_d||_2 = 1$ as

$$\mathbf{u}_{RMS} \leq J_c \tag{17}$$

and $J_c \rightarrow ||C(q)||_2$ as $M \rightarrow \infty$

Remark 3: The LSR is employed for the proposed metric because it applies to both LTI and LTV controllers [32]. Moreover, the LSR is applicable to feedforward as well as feedback controllers, SISO as well as MIMO controllers. Thus, the proposed metric is broadly applicable to any linear discrete-time tracking controller. It can also be used for evaluating other performance criteria beyond tracking accuracy and control effort.

3.2. Effect of Basis Functions on the Tracking Performance of FBF

Proposition 1: The metric of Eq. (13) applied to the FBF error dynamics (i.e., $J_{e,FBF}$) is given by

$$J_{e,FBF} = \sqrt{1 - \frac{n+1}{M+1}} \tag{18}$$

Proof: The filtered basis functions matrix $\tilde{\mathbf{\Phi}}$ in Eq. (8) can be transformed to the decoupled filtered basis functions matrix $\tilde{\mathbf{\Psi}}$ using transformation $\mathbf{\Omega}$ (for more details, see [15])

$$\begin{aligned} \tilde{\mathbf{\Phi}} &= \tilde{\mathbf{\Psi}}\mathbf{\Omega} \\ \mathbf{\Phi} &= \mathbf{\Psi}\mathbf{\Omega} \end{aligned} \tag{19}$$

such that

$$\begin{aligned} &\tilde{\mathbf{\Psi}}^{\mathrm{T}}\tilde{\mathbf{\Psi}} = \mathbf{I}_{n+1}; \\ &\mathbf{C}_{FBF} = \mathbf{\Psi}\tilde{\mathbf{\Psi}}^{\mathrm{T}}; \\ &\mathbf{E}_{ff,FBF} = \mathbf{I}_{M+1} - \tilde{\mathbf{\Psi}}\tilde{\mathbf{\Psi}}^{\mathrm{T}} \end{aligned} \tag{20}$$

Based on Eq. (20) (for more details see prior work [15]), it is known that $\mathbf{L}_{FBF}$, which depends on the selected basis functions and the plant dynamics, can be expressed as

$$\mathbf{L}_{FBF} = \sum_{i=1}^{n+1} \tilde{\boldsymbol{\psi}}_i \tilde{\boldsymbol{\psi}}_i^{\mathrm{T}} \tag{21}$$

where $\tilde{\boldsymbol{\psi}}_i$ are the decoupled filtered basis functions that satisfy

$$\begin{aligned} &\tilde{\boldsymbol{\psi}}_i^{\mathrm{T}} \tilde{\boldsymbol{\psi}}_j = \delta_{ij} \\ &\delta_{ij} = \begin{cases} 1 & i = j \\ 0 & i \neq j \end{cases} \end{aligned} \tag{22}$$

Hence,

$$\begin{aligned} J_{e,FBF} &= \frac{\left\| \mathbf{I} - \mathbf{L}_{FBF} \right\|_F}{\sqrt{M+1}} \\ &= \frac{\left\| \sum_{i=1}^{M+1} \tilde{\boldsymbol{\psi}}_i \tilde{\boldsymbol{\psi}}_i^{\mathrm{T}} - \sum_{i=1}^{n+1} \tilde{\boldsymbol{\psi}}_i \tilde{\boldsymbol{\psi}}_i^{\mathrm{T}} \right\|_F}{\sqrt{M+1}} \\ &= \frac{\left\| \sum_{i=n+2}^{M+1} \tilde{\boldsymbol{\psi}}_i \tilde{\boldsymbol{\psi}}_i^{\mathrm{T}} \right\|_F}{\sqrt{M+1}} \\ &= \sqrt{\frac{M-n}{M+1}} \\ &= \sqrt{1 - \frac{n+1}{M+1}} \end{aligned} \tag{23}$$

(End of proof)

Remark 4: Note that $J_{e,FBF}$ is independent of $G(q)$ and the type of basis functions employed. It depends only on the number of basis functions (relative to the number of discrete points in the trajectory). As discussed in [25], the independence of J_e from $G(q)$ cannot be taken for granted with other tracking controllers [26]. The consistent tracking accuracy of FBF stems from the unique structure of $\mathbf{E}_{ff,FBF}$ and it provides an analytical explanation of the relative independence of the FBF method's tracking accuracy from $G(q)$ observed in prior

work [15,17,21], and demonstrated in Section 2.3. Also, the result of Proposition 1 holds for any linear plant dynamics, i.e., it also applies to LTV and LPV plants.

Remark 5: Note that, $\|\mathbf{E}_{ff,FBF}\|_2$ is equal to 1, irrespective of the number of basis functions used, which is not a reasonable representation of the tracking accuracy of the FBF method, which varies significantly with n [15,17,21]. Hence, the proposed metric is more appropriate compared to 2-norm metrics like those used in convergence analysis in ILC [30].

Remark 6: $J_e = 0$ implies $\mathbf{C} = \mathbf{G}^{-1}$ which might be undesirable if $G(q)$ contains uncancellable zero(s) because such zeros result in very small singular values of **G,** and large control signals [33]. The FBF approach is rank constrained minimization of the metric applied to error dynamics [25]. A rank constraint, which in the LSR implies a restricted space of input and output [15], is used to avoid inversion of the full **G**, while also reducing the computational demands of the control problem [22,34,35]. However, the rank constraint does not necessarily result in minimization of control input and hence, analysis of FBF controller dynamics (discussed in the remainder of this section) and selection of an optimal set of basis functions (presented in Sec. 3.3) is necessary.

The LSR of the plant, **G**, can be decomposed using singular value decomposition (SVD) [36] as follows

$$\begin{aligned}
&\mathbf{G} = \mathbf{V}\boldsymbol{\Sigma}\mathbf{W}^{\mathrm{T}} = \sum_{i=1}^{M+1} \sigma_i \mathbf{v}_i \mathbf{w}_i^{\mathrm{T}};\\
&\mathbf{V} = \begin{bmatrix} \mathbf{v}_1 & \mathbf{v}_2 & \dots & \mathbf{v}_{M+1} \end{bmatrix};\\
&\mathbf{W} = \begin{bmatrix} \mathbf{w}_1 & \mathbf{w}_2 & \dots & \mathbf{w}_{M+1} \end{bmatrix};\\
&\boldsymbol{\Sigma} = diag\left(\begin{bmatrix} \sigma_1 & \sigma_2 & \dots & \sigma_{M+1} \end{bmatrix}\right);\\
&\sigma_1 > \sigma_2 > \ldots > \sigma_{M+1} > 0
\end{aligned} \tag{24}$$

Without loss of generality, this paper assumes that **G** has distinct singular values.

The Frobenius norm of $\mathbf{C}_{FBF}$ can be expressed as

$$\begin{aligned}\left\|\mathbf{C}_{FBF}\right\|_F &= \sqrt{trace(\mathbf{C}_{FBF}^{\mathrm{T}}\mathbf{C}_{FBF})} = \sqrt{trace(\tilde{\mathbf{\Psi}}\mathbf{\Psi}^{\mathrm{T}}\mathbf{\Psi}\tilde{\mathbf{\Psi}}^{\mathrm{T}})} \\ &= \sqrt{trace(\mathbf{\Psi}^{\mathrm{T}}\mathbf{\Psi}\tilde{\mathbf{\Psi}}^{\mathrm{T}}\tilde{\mathbf{\Psi}})} = \sqrt{trace(\mathbf{\Psi}^{\mathrm{T}}\mathbf{\Psi})} \\ &= \left\|\mathbf{\Psi}\right\|_F \\ &= \left\|\mathbf{G}^{-1}\tilde{\mathbf{\Psi}}\right\|_F = \left\|\mathbf{W}\mathbf{\Sigma}^{-1}\mathbf{V}^{\mathrm{T}}\tilde{\mathbf{\Psi}}\right\|_F = \left\|\mathbf{\Sigma}^{-1}\mathbf{V}^{\mathrm{T}}\tilde{\mathbf{\Psi}}\right\|_F \\ &= \left\|\mathbf{\Sigma}^{-1}\tilde{\mathbf{\Xi}}\right\|_F\end{aligned} \tag{25}$$

where

$$\begin{aligned}&\tilde{\mathbf{\Xi}} = \mathbf{V}^{\mathrm{T}}\tilde{\mathbf{\Psi}} \\ &\tilde{\mathbf{\Xi}} = \begin{bmatrix} \tilde{\xi}_{10} & \tilde{\xi}_{11} & \cdots & \tilde{\xi}_{1n} \\ \tilde{\xi}_{20} & \tilde{\xi}_{21} & \cdots & \tilde{\xi}_{2n} \\ \vdots & \vdots & \ddots & \vdots \\ \tilde{\xi}_{M+1,0} & \tilde{\xi}_{M+1,1} & \cdots & \tilde{\xi}_{M+1,n} \end{bmatrix} \\ &\tilde{\mathbf{\psi}}_j = \sum_{i=1}^{M+1} \tilde{\xi}_{ij}\mathbf{v}_i\end{aligned} \tag{26}$$

The implication is that $\tilde{\xi}_{ij}$ represents the contribution of $\mathbf{v}_i$ towards $\tilde{\mathbf{\psi}}_j$ and vice-versa. Hence,

$$J_{c,FBF} = \frac{\left\|\mathbf{C}_{FBF}\right\|_F}{\sqrt{M+1}} = \sqrt{\frac{1}{M+1}\sum_{i=1}^{M+1}\frac{1}{\sigma_i^2}\left(\sum_{j=0}^{n}\tilde{\xi}_{ij}^2\right)} \tag{27}$$

Since, $\mathbf{v}_i$ and $\tilde{\mathbf{\psi}}_j$ are unitary vectors

$$\begin{aligned}&\left|\tilde{\xi}_{ij}\right| \le 1 \\ &\Rightarrow \tilde{\xi}_{ij}^2 \le \left|\tilde{\xi}_{ij}\right| \\ &\Rightarrow \sum_{j=0}^{n}\tilde{\xi}_{ij}^2 \le \sum_{j=0}^{n}\left|\tilde{\xi}_{ij}\right| \le \left\|\tilde{\mathbf{\Xi}}\right\|_\infty \le \left\|\tilde{\mathbf{\Xi}}\right\|_2\end{aligned} \tag{28}$$

Based on Eqs. (20) and (26)

$$\begin{aligned} &\left\|\tilde{\boldsymbol{\Xi}}\right\|_2 = 1 \\ &\Rightarrow \sum_{j=0}^{n} \tilde{\xi}_{ij}^2 \le 1 \end{aligned} \tag{29}$$

The squared Frobenius norm of FBF controller dynamics $\left\|\mathbf{C}_{FBF}\right\|_F^2$ is a linear combination of the inverse of squared singular values of **G**, i.e., $\left\{1/\sigma_i^2\right\}_{i=1}^{M+1}$ with coefficients of the linear combination $\sum_{j=0}^{n} \tilde{\xi}_{ij}^2$ determined by interaction between filtered basis functions $\tilde{\boldsymbol{\psi}}_j$ and system dynamics **G**. The coefficients are bounded between 0 and 1 and need to satisfy orthogonality condition (see Eq. (20)).

3.3. Optimal Selection of Basis Functions for Minimal Control Effort

It has been shown, so far, that the tracking accuracy of the FBF method (measured by J_e) is always fixed for a given number of basis functions, irrespective of the type of basis functions or the plant dynamics. Also, for a given number of basis functions, the control effort of the FBF method (measured by J_c) is dependent on the plant dynamics and type of basis functions. In this section, the optimal set of basis functions that minimizes J_c for a given J_e are presented – and the resulting controller is called the optimal FBF controller (i.e., optimal in terms of minimizing control effort).

***Proposition 2*:** For n+1 basis functions, the minimum value of the squared Frobenius norm of LSR of FBF controller dynamics, $\left\|\mathbf{C}_{FBF}\right\|_F^2$, is given by

$$\min\left(\left\|\mathbf{C}_{FBF}\right\|_F^2\right) = \sum_{i=1}^{n+1} \frac{1}{\sigma_i^2} \tag{30}$$

Proof: Proposition 2 is substantiated by

- proving by contradiction that there is no $\tilde{\xi}_{ij}$ such that

$$\left\|\mathbf{C}_{FBF}\right\|_F^2 < \sum_{i=1}^{n+1} \frac{1}{\sigma_i^2} \tag{31}$$

- showing there exists $\tilde{\xi}_{ij}$ such that

$$\left\|\mathbf{C}_{FBF}\right\|_F^2 = \sum_{i=1}^{n+1} \frac{1}{\sigma_i^2} \tag{32}$$

Assume

$$\begin{aligned} &\left\|\mathbf{C}_{FBF}\right\|_F^2 = \sum_{i=1}^{M+1} \frac{1}{\sigma_i^2} \chi_i < \sum_{i=1}^{n+1} \frac{1}{\sigma_i^2}; \\ &\chi_i = \sum_{j=0}^{n} \tilde{\xi}_{ij}^2 \le 1 \end{aligned} \tag{33}$$

Therefore,

$$\sum_{i=n+2}^{M+1} \frac{1}{\sigma_i^2} \chi_i < \sum_{i=1}^{n+1} \frac{1}{\sigma_i^2} (1-\chi_i) \tag{34}$$

From Eqs. (20) and (26),

$$trace(\tilde{\mathbf{\Xi}}^{\mathrm{T}} \tilde{\mathbf{\Xi}}) = \sum_{i=1}^{M+1} \chi_i = n+1 = trace(\mathbf{I}_{n+1}) \tag{35}$$

Hence,

$$\sum_{i=n+2}^{M+1} \chi_i = \sum_{i=1}^{n+1} (1-\chi_i) \tag{36}$$

Multiplying Eq. (34) by σ_{n+1}^2 gives

$$\sum_{i=n+2}^{M+1} \frac{\sigma_{n+1}^2}{\sigma_i^2} \chi_i < \sum_{i=1}^{n+1} \frac{\sigma_{n+1}^2}{\sigma_i^2} (1-\chi_i) \tag{37}$$

Subtracting Eq. (36) from Eq. (37) results in

$$\sum_{i=n+2}^{M+1} \left(\frac{\sigma_{n+1}^2}{\sigma_i^2} - 1 \right) \chi_i < \sum_{i=1}^{n+1} \left(\frac{\sigma_{n+1}^2}{\sigma_i^2} - 1 \right) (1-\chi_i) \tag{38}$$

Note that

$$\left(\frac{\sigma_{n+1}^2}{\sigma_i^2}-1\right)>0 \quad \text{for} \quad i=n+2,n+3,\ldots M+1$$
$$\left(\frac{\sigma_{n+1}^2}{\sigma_i^2}-1\right)\le 0 \quad \text{for} \quad i=1,2,\ldots,n+1 \tag{39}$$
$$\chi_i \ge 0$$
$$(1-\chi_i)\ge 0$$

which implies that left hand side of Eq. (38) is always greater than or equal to zero whereas, the right hand side is always less than or equal to zero, which is a contradiction and hence, the assumption given by Eq. (33) is incorrect.

The minimum value of Eq. (30)

$$\left\|\mathbf{C}_{FBF}\right\|_F^2=\sum_{i=1}^{n+1}\frac{1}{\sigma_i^2} \tag{40}$$

can be realized when

$$\tilde{\xi}_{ij}=\begin{cases}\pm 1 & i=j+1, 0\le j\le n\\ 0 & \text{otherwise}\end{cases} \tag{41}$$

and hence,

$$\left\|\mathbf{C}_{FBF}\right\|_F^2\ge\sum_{i=1}^{n+1}\frac{1}{\sigma_i^2} \tag{42}$$

The minimum can be achieved at

$$\tilde{\boldsymbol{\psi}}_i=\pm\mathbf{v}_i$$
$$\boldsymbol{\psi}_i=\pm\frac{\mathbf{w}_i}{\sigma_i} \tag{43}$$
$$i=1,2,\ldots,n+1$$

The implication is that the decoupled filtered basis functions $\tilde{\boldsymbol{\psi}}_i$ are the left singular vectors (SV) of the LSR of the plant, **G**. Hence, the minimum value of metric $J_{c,FBF}$ is given by

$$\min J_{c,FBF} = \min \frac{\left\| \mathbf{C}_{FBF} \right\|_F}{\sqrt{M+1}} = \sqrt{\frac{1}{M+1} \sum_{i=1}^{n+1} \frac{1}{\sigma_i^2}} \tag{44}$$

(End of proof)

For $n = M$, i.e., the number of basis functions equals the number of trajectory points, the value of J_e and J_c are independent of the choice of basis functions and given by

$$\begin{aligned} J_e &= 0 \\ J_c &= \sqrt{\frac{1}{M+1} \sum_{i=1}^{M+1} \frac{1}{\sigma_i^2}} \end{aligned} \tag{45}$$

However, when $n = M$, the control input is undesirably high if system G contains NMP zero(s) [16,33].

Remark 7: The singular vectors (SV) based basis functions (given by Eq. (43)) are the optimal set of basis functions which result in minimum J_c for given J_e. Note that these optimal basis functions are system dependent. Inversion of the LSR, $\mathbf{G}^{-1}$ for NMP systems can be realized, approximately, by truncating the smallest singular values from the SVD of $\mathbf{G}$ [16,33]. The truncated SVD-based approximation of $\mathbf{G}^{-1}$ is a special case of the optimal FBF controller (i.e., it uses the SVs of $\mathbf{G}$ as basis functions with $n = M-r$, where r is the number of NMP zero(s) of system G).

Remark 8: For FBF, the fact that J_e is independent of plant dynamics and basis functions, whereas, J_c is dependent on the plant dynamics and basis functions permits a sequential two-stage design procedure for achieving the optimal FBF controller. In the first stage, the user selects the number of basis functions (n+1) to achieve a desired level of tracking accuracy (J_e). Then, in the second stage, the control effort (J_c) is minimized by selecting n+1 of the highest M+1−r SV components of $\mathbf{G}$ as the optimal set of basis functions.

Remark 9: While the proposed two-step methodology is general in that it is independent of desired trajectory, it can accommodate special cases where information (e.g., frequency spectrum) of a specific desired trajectory to be tracked is available. For instance, the dynamics can be pre-multiplied with a weighting filter that emphasizes the frequency content of the desired trajectory and the proposed methodology can be applied to the augmented dynamics.

Remark 10: The optimization based methodology discussed in this section can easily be extended to other control objectives (e.g., basis functions selection in presence of uncertainty) and other applications (e.g., basis functions selection for ILC).

4. EXAMPLES

4.1. Simulations

Section 2.3 motivated Sec. 3 using a first order plant and three different basis functions, viz., discrete cosine transform (DCT), block pulse functions (BPF) and B-splines. This section continues with the same example and compares the three basis functions mentioned above, with the optimal basis functions proposed in Sec. 3.3. The desired trajectory and other parameters ($M = 1000$, $n = 990$) are same as Sec. 2.3.

Figure 3 plots J_e and J_c for different basis functions and Fig. 4 plots the normalized tracking error $\mathbf{e}_{RMS}/\mathbf{y}_{d,RMS}$ and normalized control input $\mathbf{u}_{RMS}/\mathbf{y}_{d,RMS}$. Note that Figs. 3 and 4 validate the discussion in Sec. 3. The trend for $\mathbf{e}_{RMS}/\mathbf{y}_{d,RMS}$ and $\mathbf{u}_{RMS}/\mathbf{y}_{d,RMS}$ in Fig. 4 are quite similar to those of J_e and J_c, respectively, in Fig. 3, which demonstrates the effectiveness of the proposed metric. Note that there might be instances when performance trends may not exactly follow the predictions of J_e or J_c. For example, FBF might have

much better tracking accuracy than predicted by J_e or smaller control effort than predicted by J_c if one purposely (or accidentally) uses filtered basis functions that span the desired trajectory (y_d). However, in general, the proposed metric provides good insights on the upper limits of RMS tracking performance and control effort. As discussed in Sec 3.2, all the four basis functions have similar tracking error (see Fig. 4 (a)) but different control efforts (see Fig. 4 (b)). Table 1 shows the mean values of $\mathbf{e}_{RMS}/\mathbf{y}_{d,RMS}$ and $\mathbf{u}_{RMS}/\mathbf{y}_{d,RMS}$ over all a. For $\mathbf{e}_{RMS}/\mathbf{y}_{d,RMS}$, the values of the mean for different basis functions are of the same order of magnitude. This validates the discussion about consistent tracking accuracy of the FBF approach, as compared to popular methods in the literature (see Figs. 12 and 13 in Appendix C for a comparison with two such popular methods, viz. ZPETC and TS), for different types of basis functions. However, when it comes to $\mathbf{u}_{RMS}/\mathbf{y}_{d,RMS}$, the value of the mean for B-splines is four orders of magnitude higher than the value of the mean for DCT and the value of the mean for DCT is two orders of magnitude higher than BPF and optimal basis functions. Although BPF and optimal basis functions have similar order of magnitude, the value for optimal is 10% lower than the value for BPF. The example demonstrates the effectiveness of the optimal basis functions, proposed in Sec. 3.3, in tracking the desired trajectory with minimal control effort.

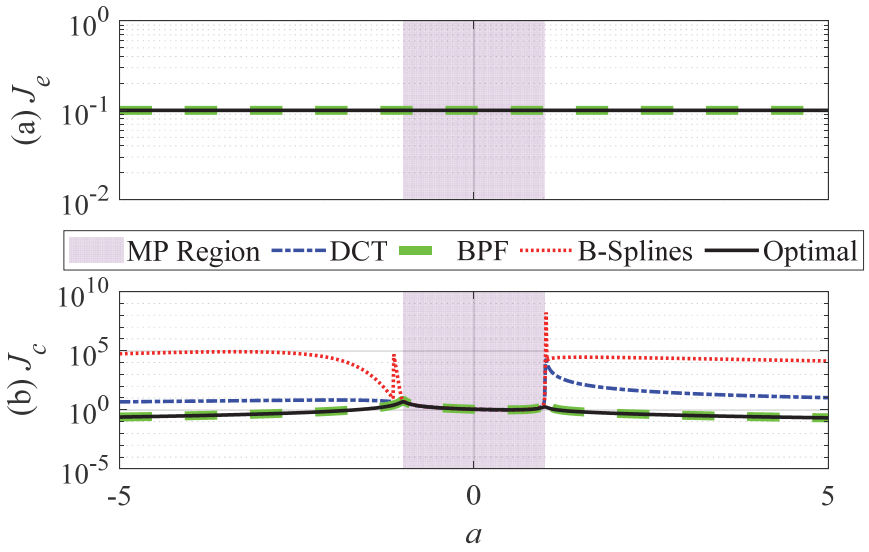

Fig. 3: Effect of basis functions (DCT, BPF, B-splines and Optimal) on (a) J_e and (b) J_c for various values of a (M = 1000, n = 990).

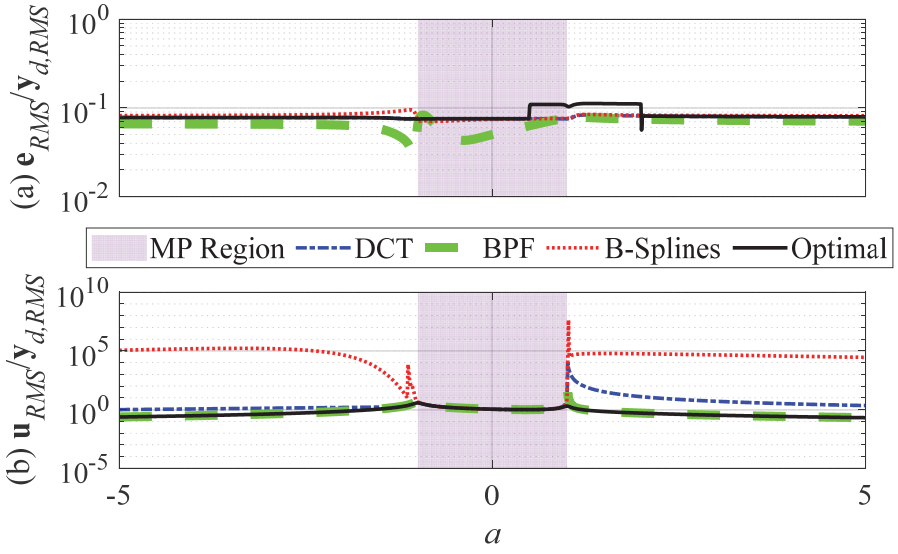

Fig. 4: Effect of basis functions (DCT, BPF, B-splines and Optimal) on (a) normalized RMS tracking error and (b) normalized RMS control input for various values of a (M = 1000, n = 990).

Tab. 1: Mean values of $\mathbf{e}_{RMS}/\mathbf{y}_{d,RMS}$ and $\mathbf{u}_{RMS}/\mathbf{y}_{d,RMS}$ over all a for different basis functions

Attribute	DCT	BPF	B-splines	Optimal
$\mathbf{e}_{RMS}/\mathbf{y}_{d,RMS}$	7.83×10^{-2}	6.62×10^{-2}	8.14×10^{-2}	8.28×10^{-2}
$\mathbf{u}_{RMS}/\mathbf{y}_{d,RMS}$	2.76×10^{1}	7.84×10^{-1}	1.02×10^{5}	7.06×10^{-1}

4.2. Experiments

This section demonstrates the practical benefits of optimal basis function selection in experiments. The biaxial (X-Y) linear motor driven stage (Aerotech ALS 25010), shown in Fig. 5, is used for the experiments. The stage is controlled using a P/PI feedback controller, augmented with velocity and acceleration feedforward [37] (see Fig. 6). The controller is implemented on a dSPACE 1202 real-time control board with 10 kHz sampling frequency. A flexible fixture consisting of a block mounted on a slender rod is attached to the stage. The block is assumed to represent an apparatus, for example, a tool, a workpiece or a measurement device whose position needs to be tracked accurately despite its flexible structure. The FBF approach is used as a feedforward tracking controller as shown in the block diagram of Fig. 6. The FBF approach takes in the desired position commands y_d for each axis and generates modified position commands u that are sent to the stage to ensure that the actual position of the block y follows y_d accurately, in spite of its inherent structural flexibilities. The actual position of the block is observed from its

accelerations measured using two unidirectional accelerometers (PCB piezotronics 393B05).

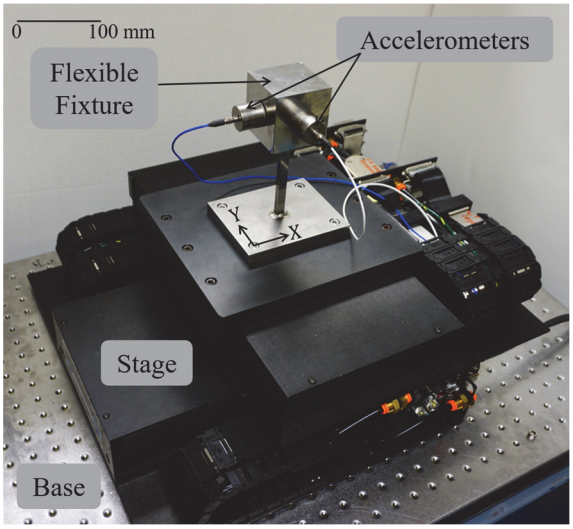

Fig. 5: Biaxial stage with flexible fixture

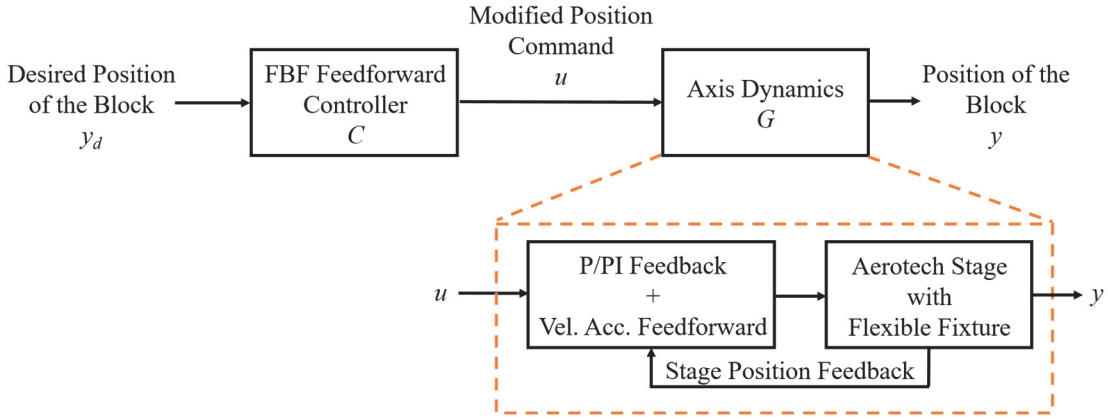

Fig. 6: Block diagram of the FBF controller and experimental setup

Figure 7 shows the frequency response function (FRF) of the dynamics of each axis of the stage, generated by applying swept sine acceleration inputs to the stage and measuring the corresponding accelerations of the block using the accelerometers. Each axis has 4 modes (two dominant and two less dominant) and hence, the plant dynamics is eighth-order. Prior work of the authors [38] provides more details about a continuous-time model

for the system, which indicates the presence of one NMP zero in the dynamics of each axis. The Markov parameters of the dynamics are obtained from the continuous-time model and are used to construct a finite impulse response (FIR) representation of the dynamics along each axis. Figure 7 shows a good match between the measured FRF and the FRF generated using the FIR representations (modeled). Based on the methodology discussed in Appendix A, the LSR of the dynamics of each axis is generated using the FIR representation. Singular values of the LSRs (for $M = 10000$) are shown in Fig. 8. Note that each axis has two very small singular values which deviate from the cluster and these singular values result in large control inputs, if the basis functions are not properly selected. One of the two singular values along each axis arises from the NMP zero, whereas, the other small singular value is a result of relative degree of one (the first Markov parameter is zero). Figure 9 shows the desired butterfly shaped path, whereas Fig. 10 show the desired paths position along the X and Y axes (for more details see [38]). The duration of the trajectory is 1 second (i.e., $M = 10000$, based on 10 kHz sampling frequency).

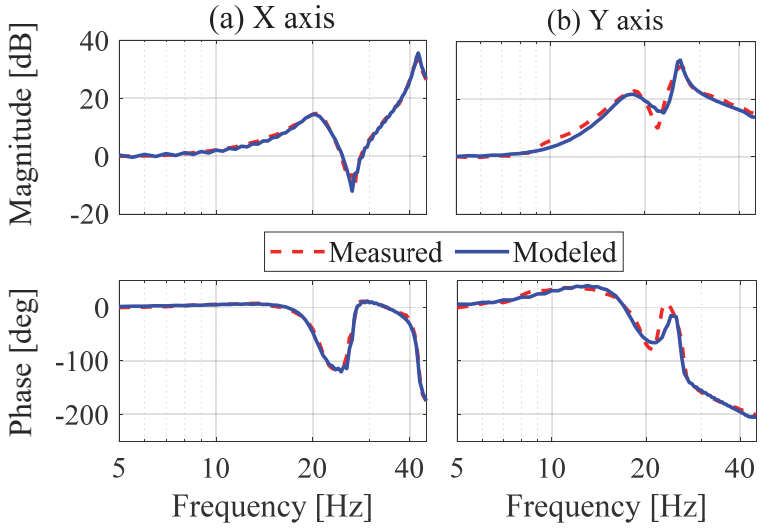

Fig. 7: Measured and modeled frequency response functions of the X and Y axes of the biaxial stage

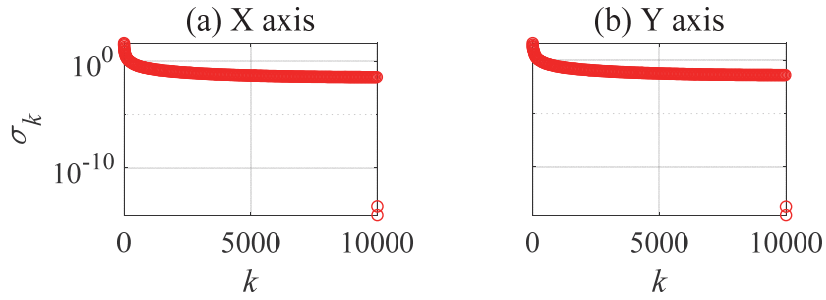

Fig. 8: Singular values of the LSRs of the X and Y dynamics

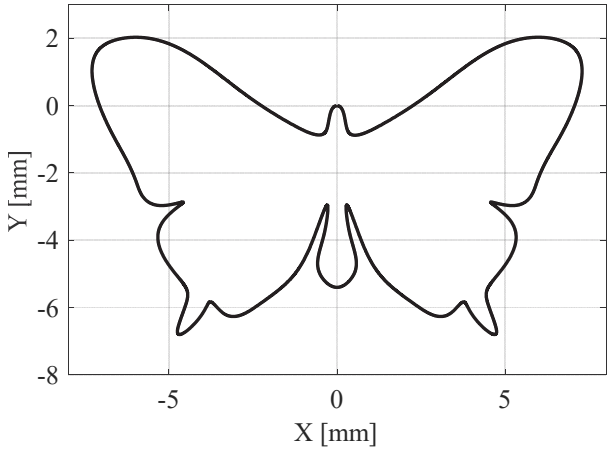

Fig. 9: Desired path

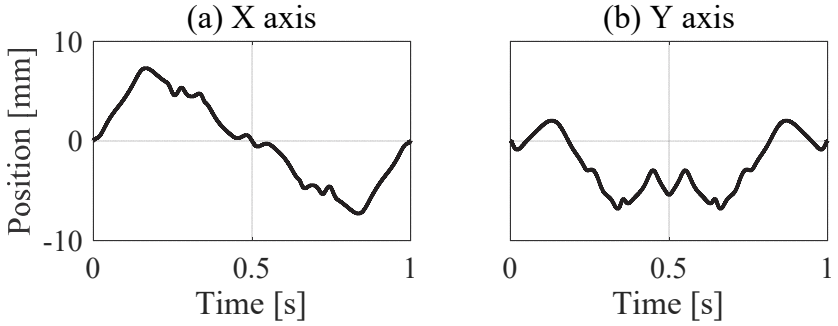

Fig. 10: Desired position trajectories along the X and Y axes

For experiments, the optimal basis functions proposed in the paper are compared with B-splines, because they are often the basis functions of choice for manufacturing and robotics applications [12,17,21,28,38]. Figure 11 shows the control input (i.e., modified position commands) sent to the X and Y axes for the two sets of basis functions (for n =

600). Also, shown are the resultant tracking errors, which are based on position signals derived from measured acceleration signals using an observer. Note that the B-spline based control input show rapid growth in magnitude towards the end of the signal because of the small singular values of the LSR corresponding to the NMP zero and the relative degree. For safety reasons, a limit ± 10 mm is placed on the position commands for both axes, as shown in Fig. 11; the B-spline control input saturates at the limit. Notice that, before saturation, the control inputs for the proposed optimal basis functions and B-splines are quite similar which results in similar tracking errors. In the time interval between 0 and 0.99 s, the RMS tracking errors for optimal basis functions and B-splines are 263.31 μm and 250.85 μm, respectively, for the X-axis and between 0 and 0.96 s, 171.29 μm and 186.12 μm, respectively, for the Y-axis. However, because of saturation, the B-spline based commands generate large tracking errors, as shown in Fig. 11. Consequently, the overall RMS tracking error for B-splines, along the X and Y axes, are respectively 3 and 19 times the RMS tracking error for the optimal basis functions (see Tab. 2). Moreover, the optimal basis functions require 3% and 13% lower control effort than B-splines for X-axis and Y-axis, respectively. The proposed optimal basis functions track much better than B-splines and require less control effort.

Remark 11: The violation of actuator limits by B-splines observed in the results of Fig. 11 can be mitigated by formulating the FBF approach as a constrained optimization problem using the constraint handling capabilities of B-splines, as done in prior work of the authors [38]. However, all things being equal, it is theoretically and practically preferable to avoid large control signals altogether than to contain them via constraints.

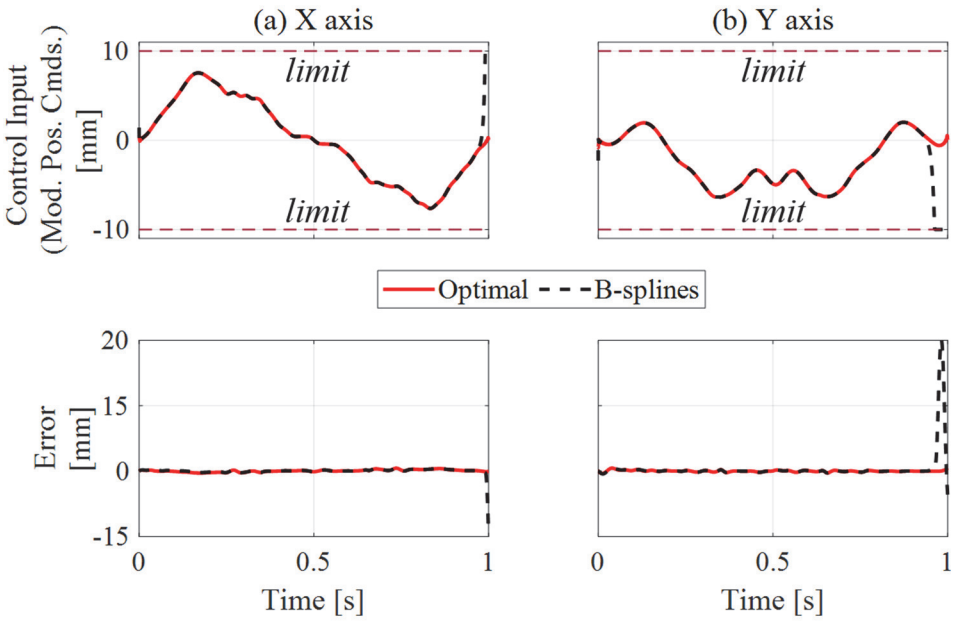

Fig. 11: X and Y control inputs (i.e., modified position command) signals and tracking errors for optimal basis functions and B-splines (M = 10000, n = 600)

Tab. 2: Summary of tracking error and control effort for experiments

Basis Functions	X axis		Y axis	
	$\mathbf{e}_{RMS}/\mathbf{y}_{d,RMS}$	$\mathbf{u}_{RMS}/\mathbf{y}_{d,RMS}$	$\mathbf{e}_{RMS}/\mathbf{y}_{d,RMS}$	$\mathbf{u}_{RMS}/\mathbf{y}_{d,RMS}$
Optimal	0.06	1.05	0.05	0.98
B-Splines	0.17	1.08	0.94	1.12

5. CONCLUSIONS AND FUTURE WORK

An appealing feature of the FBF approach is that it provides a control engineer with a wide variety of basis functions for use in tracking control (of NMP systems). However, to date, there has been no work on how to determine the best set of basis functions to achieve a given tracking control objective. To address this shortcoming, this paper has

proposed a methodology for optimal selection of basis functions that minimize control effort of the FBF controller without sacrificing its tracking accuracy.

To facilitate optimal basis functions selection, a new metric based on the Frobenius norm of the LSR of system dynamics is proposed. The proposed metric is versatile. It is useful for analyzing and evaluating the performance of any linear discrete-time controller (including LTV controllers like FBF) independent of the inputs to the controller, in a manner akin to the use of Bode plots for LTI systems. It is shown that, for FBF, the proposed metric applied to tracking error dynamics is independent of the plant dynamics and type of basis functions; it depends only on the number of basis functions, relative to the length of the trajectory to be tracked. This finding is remarkable because it provides a theoretical justification for observations made by the authors in prior work about the unusual consistency of the tracking accuracy of the FBF approach irrespective of system dynamics and basis functions. Conversely, the metric shows that the control effort of the FBF approach depends on basis functions and plant dynamics.

Leveraging the analysis, a two-step process for selecting optimal basis functions that minimize control effort for a specified tracking accuracy is proposed. In the first step, the number of basis functions is selected to satisfy a desired level of tracking accuracy regardless of the type of basis functions; in the second step, the optimal set of basis functions – which are related to the singular vectors of the controlled system – are determined for minimum control effort. Simulations and experiments are used to demonstrate the effectiveness of the proposed optimal basis functions. Simple first-order plants with varying zero locations in the z-plane are used in simulations and the proposed basis functions are compared with three other commonly used basis functions (DCT, BPF

and B-splines). The results demonstrate the effectiveness of the proposed metric as well as the superiority of the optimal basis functions. Experiments on an Aerotech linear motor driven stage, with a flexible structure, are used to show that the proposed basis functions can effectively track a desired trajectory with minimal effort, as compared to B-splines which require much higher control effort, resulting in control saturation and degradation of tracking accuracy.

This study demonstrates the importance of a systematic approach for optimally selecting basis functions not only for the FBF approach but also for related control techniques, like iterative learning control, where basis functions are commonly used and often selected in an ad hoc manner. Ongoing work has focused on design of robust FBF controllers [39,40]. Future work will investigate the use of the proposed metric to study selection of basis functions to enhance the robustness of the FBF approach in presence of model uncertainties. The use of the proposed metric as a tool to analyze and design other optimal linear discrete-time controllers beyond the FBF approach will also be explored.

FUNDING

This work is partially funded by the National Science Foundation – CMMI 1825133: Boosting the Speed and Accuracy of Vibration-Prone Manufacturing Machines at Low Cost through Software

REFERENCES

[1] Tomizuka, M., 1987, “Zero Phase Error Tracking Algorithm for Digital Control,” J. Dyn. Syst. Meas. Control, **109**(1), pp. 65–68.

[2] Torfs, D., De Schutter, J., and Swevers, J., 1992, "Extended Bandwidth Zero Phase Error Tracking Control of Nonminimal Phase Systems," J. Dyn. Syst. Meas. Control, **114**(3), pp. 347–351.

[3] Gross, E., Tomizuka, M., and Messner, W., 1994, "Cancellation of Discrete Time Unstable Zeros by Feedforward Control," J. Dyn. Syst. Meas. Control, **116**(1), pp. 33–38.

[4] Devasia, S., Chen, D., and Paden, B., 1996, "Nonlinear Inversion-Based Output Tracking," Autom. Control. IEEE Trans., **41**(7), pp. 930–942.

[5] Hunt, L., Meyer, G., and Su, R., 1996, "Noncausal Inverses for Linear Systems," Autom. Control. IEEE Trans., **41**(4), pp. 608–611.

[6] Zou, Q., and Devasia, S., 1999, "Preview-Based Stable-Inversion for Output Tracking of Linear Systems," J. Dyn. Syst. Meas. Control, **121**(4), pp. 625–630.

[7] Marconi, L., Marro, G., and Melchiorri, C., 2001, "A Solution Technique for Almost Perfect Tracking of Non-Minimum-Phase, Discrete-Time Linear Systems," Int. J. Control, **74**(5), pp. 496–506.

[8] Kwon, D.-S., and Book, W. J., 1994, "A Time-Domain Inverse Dynamic Tracking Control of a Single-Link Flexible Manipulator," J. Dyn. Syst. Meas. Control, **116**(2), p. 193.

[9] Trautt, T. A., and Bayo, E., 1997, "Inverse Dyamics of Non-Minimum Phase Systems with Non-Zero Initial Conditions," Dyn. Control, **7**(1), pp. 49–71.

[10] Rigney, B. P., Pao, L. Y., and Lawrence, D. A., 2009, "Nonminimum Phase Dynamic Inversion for Settle Time Applications," Control Syst. Technol. IEEE Trans., **17**(5), pp. 989–1005.

[11] Wen, J. T., and Potsaid, B., 2004, "An Experimental Study of a High Performance Motion Control System," *American Control Conference, 2004. Proceedings of the 2004*, pp. 5158–5163.

[12] Wang, H., Kim, K., and Zou, Q., 2013, "B-Spline-Decomposition-Based Output Tracking With Preview for Nonminimum-Phase Linear Systems," Automatica, **49**(5), pp. 1295–1303.

[13] Jetto, L., Orsini, V., and Romagnoli, R., 2014, "Accurate Output Tracking for Nonminimum Phase Nonhyperbolic and Near Nonhyperbolic Systems," Eur. J. Control, **20**(6), pp. 292–300.

[14] Jetto, L., Orsini, V., and Romagnoli, R., 2015, "Spline Based Pseudo-Inversion of Sampled Data Non-Minimum Phase Systems for an Almost Exact Output Tracking," Asian J. Control, **17**(5), pp. 1866–1879.

[15] Ramani, K. S., Duan, M., Okwudire, C. E., and Ulsoy, A. G., 2017, "Tracking Control of Linear Time-Invariant Nonminimum Phase Systems Using Filtered Basis Functions," J. Dyn. Syst. Meas. Control, **139**(1), p. 011001.

[16] Ronde, M., van de Molengraft, R., and Steinbuch, M., 2012, "Model-Based Feedforward for Inferential Motion Systems, with Application to a Prototype Lightweight Motion System," *American Control Conference (ACC), 2012*, pp. 5324–5329.

[17] Duan, M., Yoon, D., and Okwudire, C. E., 2018, "A Limited-Preview Filtered B-Spline Approach to Tracking Control – with Application to Vibration-Induced Error Compensation of a Commercial 3D Printer," Mechatronics, **56**, pp. 287--296.

[18] Kasemsinsup, Y., Romagnoli, R., Heertjes, M., Weiland, S., and Butler, H., 2017,

"Reference-Tracking Feedforward Control Design for Linear Dynamical Systems through Signal Decomposition," *American Control Conference (ACC), 2017*, pp. 2387--2392.

[19] Romagnoli, R., and Garone, E., 2019, "A General Framework for Approximated Model Stable Inversion," Automatica, **101**, pp. 182–189.

[20] Frueh, J. A., and Phan, M. Q., 2000, "Linear Quadratic Optimal Learning Control (LQL)," Int. J. Control, **73**(10), pp. 832–839.

[21] Duan, M., Ramani, K. S., and Okwudire, C. E., 2015, "Tracking Control of Non-Minimum Phase Systems Using Filtered Basis Functions: A NURBS-Based Approach," *ASME 2015 Dynamic Systems and Control Conference*, American Society of Mechanical Engineers, p. V001T03A006--V001T03A006.

[22] Ye, Y., and Wang, D., 2005, "DCT Basis Function Learning Control," Mechatronics, IEEE/ASME Trans., **10**(4), pp. 449–454.

[23] Hamamoto, K., and Sugie, T., 2001, "An Iterative Learning Control Algorithm Within Prescribed Input--Output Subspace," Automatica, **37**(11), pp. 1803–1809.

[24] Bolder, J., Oomen, T., and Steinbuch, M., 2013, "Exploiting Rational Basis Functions in Iterative Learning Control," *52nd IEEE Conference on Decision and Control*, pp. 7321–7326.

[25] Ramani, K. S., Duan, M., Okwudire, C. E., and Ulsoy, A. G., 2018, "A Lifted Domain-Based Metric for Performance Evaluation of LTI and LTV Discrete-Time Tracking Controllers," *2018 International Symposium on Flexible Automation*.

[26] Butterworth, J. A., Pao, L. Y., and Abramovitch, D. Y., 2012, "Analysis and Comparison of Three Discrete-Time Feedforward Model-Inverse Control

Techniques for Nonminimum-Phase Systems," Mechatronics, **22**(5), pp. 577–587.

[27] Deb, A., Sarkar, G., and Sen, S. K., 1994, "Block Pulse Functions, the Most Fundamental of All Piecewise Constant Basis Functions," Int. J. Syst. Sci., **25**(2), pp. 351–363.

[28] Piegl, L., and Tiller, W., 1997, *The NURBS Book*, New York: Springer.

[29] Piegl, L., 1991, "On NURBS: A Survey," IEEE Comput. Graph. Appl., **11**(1), pp. 55–71.

[30] Barton, K. L., Bristow, D. A., and Alleyne, A. G., 2010, "A Numerical Method for Determining Monotonicity and Convergence Rate in Iterative Learning Control," Int. J. Control, **83**(2), pp. 219–226.

[31] Dijkstra, B. G., 2004, "Iterative Learning Control With Applications to a Wafer Stage," Doctoral Thesis, Delft University of Technology, Netherlands.

[32] Bristow, D. A., Tharayil, M., and Alleyne, A. G., 2006, "A Survey of Iterative Learning Control," IEEE Control Syst. Mag., **26**(3), pp. 96–114.

[33] Lunenburg, J., Bosgra, O., and Oomen, T., 2009, "Inversion-Based Feedforward Design for Beyond Rigid Body Systems : A Literature Survey," DCT Rep. 2009.105, Eindhoven Univ. Technol. Eindhoven, Netherlands.

[34] Phan, M., and Frueh, J., 1996, "Learning Control for Trajectory Tracking Using Basis Functions," *Decision and Control, 1996., Proceedings of the 35th IEEE Conference On*, pp. 2490–2492.

[35] Yoon, D., and Okwudire, C. E., 2016, "Active Assist Device for Simultaneous Reduction of Heat and Vibration in Precision Scanning Stages," Precis. Eng., **46**, pp. 193–205.

[36] Laub, A. J., 2005, *Matrix Analysis for Scientists and Engineers*, Siam.

[37] Altintas, Y., and Okwudire, C. E., 2009, "Dynamic Stiffness Enhancement of Direct-Driven Machine Tools Using Sliding Mode Control with Disturbance Recovery," CIRP Ann. - Manuf. Technol., **58**(1), pp. 335–338.

[38] Okwudire, C., Ramani, K., and Duan, M., 2016, "A Trajectory Optimization Method for Improved Tracking of Motion Commands Using CNC Machines That Experience Unwanted Vibration," CIRP Ann. - Manuf. Technol., **65**(1), pp. 373–376.

[39] Ramani, K. S., and Okwudire, C. E., 2016, "Regularized Filtered Basis Functions Approach for Accurate Tracking of Discrete-Time Linear Time Invariant Systems with Bounded Random Uncertainties," *ASME 2016 Dynamic Systems and Control Conference, American Society of Mechanical Engineers*.

[40] Ramani, K. S., and Okwudire, C. E., 2018, "Robust Filtered Basis Functions Approach for Feedforward Tracking Control," *ASME 2018 Dynamic Systems and Control Conference*.

[41] Oppenheim, A. V, Schafer, R. W., and Buck, J. R., 1989, *Discrete-Time Signal Processing*, Prentice-hall Englewood Cliffs.

[42] Riley, K. F., Hobson, M. P., and Bence, S. J., 2006, *Mathematical Methods for Physics and Engineering: A Comprehensive Guide*, Cambridge university press.

APPENDIX A: Lifted System Representation (LSR)

An LTI SISO causal plant G can be expressed as

$$G(q) = g_0 + g_1 q^{-1} + g_2 q^{-2} + \dots \tag{46}$$

where the coefficients g_l are the Markov parameters of G. The sequence $g_0, g_1, g_2, \dots$ also represent the impulse response of G. Then

$$\underbrace{\begin{bmatrix} y(0) \\ y(1) \\ \vdots \\ y(M) \end{bmatrix}}_{\mathbf{y}} = \underbrace{\begin{bmatrix} g_0 & 0 & \dots & 0 \\ g_1 & g_0 & \dots & 0 \\ \vdots & \vdots & \ddots & \vdots \\ g_M & g_{M-1} & \dots & g_0 \end{bmatrix}}_{\mathbf{G}} \underbrace{\begin{bmatrix} u(0) \\ u(1) \\ \vdots \\ u(M) \end{bmatrix}}_{\mathbf{u}} \tag{47}$$

For an LTI non-causal controller C

$$C(q) = \dots + c_{-2} q^2 + c_{-1} q^1 + c_0 + c_1 q^{-1} + c_2 q^{-2} + \dots \tag{48}$$

the LSR of $\boldsymbol{C}$ can be expressed as

$$\underbrace{\begin{bmatrix} u(0) \\ u(1) \\ \vdots \\ u(M) \end{bmatrix}}_{\mathbf{u}} = \underbrace{\begin{bmatrix} c_0 & c_{-1} & \dots & c_{-M} \\ c_1 & c_0 & \dots & c_{-M+1} \\ \vdots & \vdots & \ddots & \vdots \\ c_M & c_{M-1} & \dots & c_0 \end{bmatrix}}_{\mathbf{C}} \underbrace{\begin{bmatrix} y_d(0) \\ y_d(1) \\ \vdots \\ y_d(M) \end{bmatrix}}_{\mathbf{y}_d} \tag{49}$$

Similarly, overall dynamics L and error dynamics E_{ff} can be expressed in LSR as $\mathbf{L}$ and $\mathbf{E}_{ff}$. For LTI systems, the LSR is Toeplitz. For LTV systems or controllers, the construction of the LSR for L and E_{ff} follows a similar process but the resulting matrices are not Toeplitz [32].

APPENDIX B: Basis Functions

The DCT is a frequency-based transform that is widely used in signal processing; its basis functions are real-valued cosines defined as [22]

$$\varphi_i(k) = \beta_i \cos\left(\frac{\pi(2k+1)i}{2(M+1)}\right);\ \beta_i = \begin{cases} \dfrac{1}{\sqrt{M+1}} & i = 0 \\ \sqrt{\dfrac{2}{M+1}} & i > 0 \end{cases} \tag{50}$$

The BPF basis functions are given by

$$\varphi_i(k) = \begin{cases} 1 & k \in \left[i\dfrac{M}{n+1}, (i+1)\dfrac{M}{n+1} \right), 0 \le i < n \\ & \&\ k \in \left[i\dfrac{M}{n+1}, (i+1)\dfrac{M}{n+1} \right], i = n \\ 0 & \text{otherwise} \end{cases} \tag{51}$$

The BPF expressed in Eq. (51) seeks to divide the time interval from 0 to M among n+1 basis functions in a quasi-uniform manner.

For a B-spline of degree m, having $n+1 \le M+1$ control points (same as coefficients of basis functions), γ_0, γ_1, ..., γ_n, and knot vector $[\eta_0\ \eta_1\ \ldots\ \eta_{m+n+1}]^T$, its real-valued basis functions, $\varphi_{i,m}$, are given by [28]

$$\begin{aligned} \varphi_i(k) &:= \varphi_{i,m}(\xi_k) = \frac{\xi_k - \eta_i}{\eta_{i+m} - \eta_i}\varphi_{i,m-1}(\xi) + \frac{\eta_{i+m+1} - \xi_k}{\eta_{i+m+1} - \eta_{i+1}}\varphi_{i+1,m-1}(\xi) \\ \varphi_{i,0}(\xi_k) &= \begin{cases} 1 & \eta_i \le \xi_k \le \eta_{i+1} \\ 0 & \text{otherwise} \end{cases} \end{aligned} \tag{52}$$

where i = 0, 1, ..., n with $\xi_k \in [0,1]$, representing normalized time, discretized into M+1 points, ξ_0, ξ_1 …ξ_M, and η_j is a uniform knot vector, selected such that

$$\eta_j = \begin{cases} 0 & 0 \le j \le m \\ \dfrac{j-m}{n-m+1} & m+1 \le j \le n \\ 1 & n+1 \le j \le m+n+1 \end{cases} \tag{53}$$

APPENDIX C: Comparison of FBF with ZPETC and TS

This appendix compares the tracking accuracy of FBF with that of ZPETC and TS, using the normalized RMS tracking error $\mathbf{e}_{RMS}/\mathbf{y}_{d,RMS}$ (Fig. 12) and the proposed Frobenius norm metric J_e (Fig. 13), for various zero locations $a \in [-10, 10]$. The trend for J_e and $\mathbf{e}_{RMS}/\mathbf{y}_{d,RMS}$ are quite similar and agree with observations made in the literature [3,15,17,21,26]. The results show that the tracking performance of FBF is consistent as compared to popular methods in the literature, viz., ZPETC and TS. For more details, interested readers can see prior work of the authors [25].

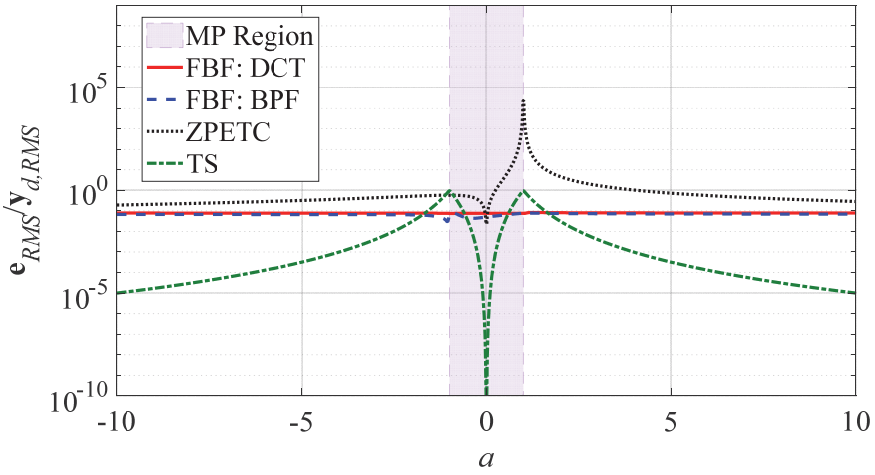

Fig. 12: Effect of zero location on normalized RMS tracking error for FBF (DCT, BPF), ZPETC and TS (for more details see [25])

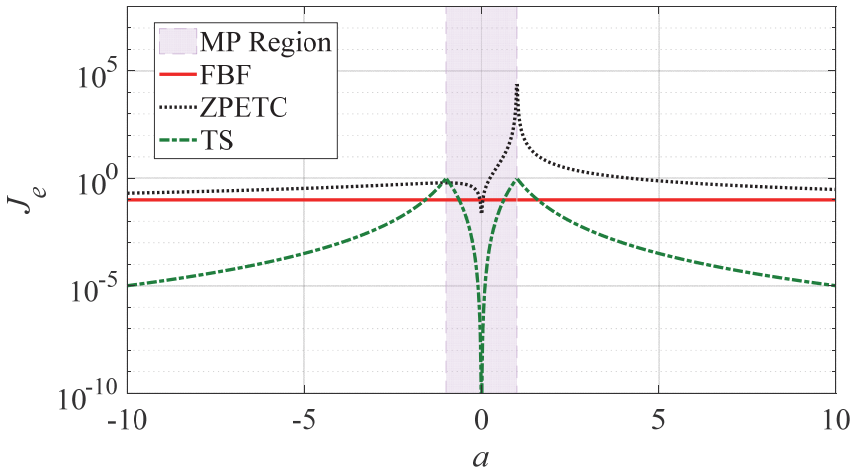

Fig. 13: Effect of zero location on Frobenius norm metric for FBF, ZPETC and TS (for more details see [25])

APPENDIX D: Relationship between Metric and System Dynamics 2-norm

Based on Appendix A, the squared Frobenius norm of the LSR of $\mathbf{E}_{ff}$ can be expressed as

$$\begin{aligned}\left\|\mathbf{E}_{ff}\right\|_F^2 &= \sum_{l=1}^{M+1}\sum_{k=l-1-M}^{l-1} e_{ff,k}^2 \\ &= e_{ff,-M}^2 + e_{ff,-M+1}^2 + \ldots + e_{ff,0}^2 \\ &+ e_{ff,-M+1}^2 + e_{ff,-M+2}^2 + \ldots + e_{ff,1}^2 \\ &+ \ldots \\ &+ e_{ff,0}^2 + e_{ff,1}^2 + \ldots + e_{ff,M}^2\end{aligned} \tag{54}$$

According to definition of 2-norm of $E_{ff}(q)$ and Parseval's Theorem [41]

$$\left\|E_{ff}(q)\right\|_2^2 = \frac{\int_0^{2\pi}\left|E_{ff}(e^{j\theta})\right|^2 d\theta}{2\pi} = \sum_{k=-\infty}^{\infty} e_{ff,k}^2 \tag{55}$$

where

$$E_{ff}(e^{j\theta}) = \sum_{k=-\infty}^{\infty} e_{ff,-k} e^{jk\theta} \tag{56}$$

Consider

$$\begin{aligned}
&(M+1)\sum_{k=-\infty}^{\infty} e_{ff,k}^2 \\
&= \sum_{l=1}^{M+1}\sum_{k=-\infty}^{\infty} e_{ff,k}^2 \\
&= \sum_{k=-\infty}^{-M-1} e_{ff,k}^2 + e_{ff,-M}^2 + e_{ff,-M+1}^2 + \ldots + e_{ff,0}^2 + \sum_{k=1}^{M} e_{ff,k}^2 + \sum_{k=M+1}^{\infty} e_{ff,k}^2 \\
&\quad + \ldots \\
&\quad + \sum_{k=-\infty}^{-M-1} e_{ff,k}^2 + \sum_{k=-M}^{h-M-2} e_{ff,k}^2 + e_{ff,h-M-1}^2 + e_{ff,h-M}^2 + \ldots + e_{ff,h-1}^2 + \sum_{k=h}^{M} e_{ff,k}^2 + \sum_{k=M+1}^{\infty} e_{ff,k}^2 \\
&\quad + \ldots \\
&\quad + \sum_{k=-\infty}^{-M-1} e_{ff,k}^2 + \sum_{k=-M}^{-1} e_{ff,k}^2 + e_{ff,0}^2 + e_{ff,1}^2 + \ldots + e_{ff,M}^2 + \sum_{k=M+1}^{\infty} e_{ff,k}^2
\end{aligned} \tag{57}$$

and using Eq. (54),

$$(M+1)\sum_{k=-\infty}^{\infty} e_{ff,k}^2 = \left\|\mathbf{E}_{ff}\right\|_F^2 + (M+1)\sum_{k=-\infty}^{-M-1} e_{ff,k}^2 + (M+1)\sum_{k=M+1}^{\infty} e_{ff,k}^2 + \sum_{k=-M}^{M} |k| e_{ff,k}^2 \tag{58}$$

Re-arrangement of the terms in the equation results in

$$\frac{\left\|\mathbf{E}_{ff}\right\|_F^2}{M+1} = \sum_{k=-\infty}^{\infty} e_{ff,k}^2 - \sum_{k=-\infty}^{-M-1} e_{ff,k}^2 - \sum_{k=M+1}^{\infty} e_{ff,k}^2 - \sum_{k=-M}^{M} \frac{|k|}{M+1} e_{ff,k}^2 \tag{59}$$

Consider two different values of M, M_1 and M_2 such that $M_1 > M_2$, then

$$\begin{aligned}
\frac{\left\|\mathbf{E}_{ff}[M_1]\right\|_F^2}{M_1+1} &= \sum_{k=-\infty}^{\infty} e_{ff,k}^2 - \sum_{k=-\infty}^{-M_1-1} e_{ff,k}^2 - \sum_{k=M_1+1}^{\infty} e_{ff,k}^2 - \sum_{k=-M_1}^{M_1} \frac{|k|}{M_1+1} e_{ff,k}^2 \\
\frac{\left\|\mathbf{E}_{ff}[M_2]\right\|_F^2}{M_2+1} &= \sum_{k=-\infty}^{\infty} e_{ff,k}^2 - \sum_{k=-\infty}^{-M_2-1} e_{ff,k}^2 - \sum_{k=M_2+1}^{\infty} e_{ff,k}^2 - \sum_{k=-M_2}^{M_2} \frac{|k|}{M_2+1} e_{ff,k}^2
\end{aligned} \tag{60}$$

where $\mathbf{E}_{ff}[M_1]$ and $\mathbf{E}_{ff}[M_2]$ denote the LSRs of $E_{ff}(q)$ for trajectory lengths M_1+1 and M_2+1, respectively. Then

$$
\begin{aligned}
&\frac{\left\|\mathbf{E}_{ff}[M_1]\right\|_F^2}{M_1+1}-\frac{\left\|\mathbf{E}_{ff}[M_2]\right\|_F^2}{M_2+1}\\
&=-\sum_{k=-\infty}^{-M_1-1}e_{ff,k}^2+\sum_{k=-\infty}^{-M_2-1}e_{ff,k}^2-\sum_{k=M_1+1}^{\infty}e_{ff,k}^2+\sum_{k=M_2+1}^{\infty}e_{ff,k}^2\\
&\quad-\sum_{k=-M_1}^{M_1}\frac{|k|}{M_1+1}e_{ff,k}^2+\sum_{k=-M_2}^{M_2}\frac{|k|}{M_2+1}e_{ff,k}^2\\
&=\sum_{k=-M_1}^{-M_2-1}e_{ff,k}^2+\sum_{k=M_2+1}^{M_1}e_{ff,k}^2-\sum_{k=-M_1}^{-M_2-1}\frac{|k|}{M_1+1}e_{ff,k}^2-\sum_{k=M_2+1}^{M_1}\frac{|k|}{M_1+1}e_{ff,k}^2\\
&\quad-\sum_{k=-M_2}^{M_2}\frac{|k|}{M_1+1}e_{ff,k}^2+\sum_{k=-M_2}^{M_2}\frac{|k|}{M_2+1}e_{ff,k}^2\\
&=\sum_{k=-M_1}^{-M_2-1}\left(1-\frac{|k|}{M_1+1}\right)e_{ff,k}^2+\sum_{k=M_2+1}^{M_1}\left(1-\frac{|k|}{M_1+1}\right)e_{ff,k}^2\\
&\quad+\sum_{k=-M_2}^{M_2}\left(\frac{1}{M_2+1}-\frac{1}{M_1+1}\right)|k|e_{ff,k}^2\\
&=\sum_{k=-M_1}^{-M_2-1}\left(1-\frac{|k|}{M_1+1}\right)e_{ff,k}^2+\sum_{k=M_2+1}^{M_1}\left(1-\frac{|k|}{M_1+1}\right)e_{ff,k}^2\\
&\quad+\sum_{k=-M_2}^{M_2}\frac{M_1-M_2}{(M_1+1)(M_2+1)}|k|e_{ff,k}^2\\
&>0
\end{aligned}
\tag{61}
$$

The implication is that for $M_1 > M_2$

$$
\frac{\left\|\mathbf{E}_{ff}[M_1]\right\|_F^2}{M_1+1}>\frac{\left\|\mathbf{E}_{ff}[M_2]\right\|_F^2}{M_2+1} \tag{62}
$$

i.e., the value of the proposed Frobenius norm metric J_e increases as M increases for a given dynamics $E_{ff}(q)$.

Combining Eqs. (55) and (59)

$$\frac{\left\|\mathbf{E}_{ff}\right\|_F^2}{M+1} = \left\|E_{ff}(q)\right\|_2^2 - \sum_{k=-\infty}^{-M-1} e_{ff,k}^2 - \sum_{k=M+1}^{\infty} e_{ff,k}^2 - \sum_{k=-M}^{M} \frac{|k|}{M+1} e_{ff,k}^2 \tag{63}$$

As $M \to \infty$, the first two summation terms on right hand side of Eq. (63) tend to 0. Assume that $e_{ff,k}$ is bounded by an exponential function, i.e.,

$$e_{ff,k}^2 \leq A e^{-\mu|k|} \tag{64}$$

where e (on the right hand side) is the Euler's number and A and μ are positive non-zero constants. The implication of the assumption is that the output of dynamics E_{ff} at a particular instant of time depends more on input at the current time instant and inputs immediately preceding or succeeding the current input as compared to inputs which occurred long time back or will occur after a long time in the future. This assumption is true for stable systems. Hence, the third summation term on right hand side of Eq. (63) is bounded by

$$\sum_{k=-M}^{M} \frac{|k|}{M+1} e_{ff,k}^2 \leq A \sum_{k=-M}^{M} \frac{|k|}{M+1} e^{-\mu|k|} \tag{65}$$

Consider the bound on the summation,

$$A \sum_{k=-M}^{M} \frac{|k|}{M+1} e^{-\mu|k|} = 2A \sum_{k=0}^{M} \frac{k}{M+1} e^{-\mu k} \tag{66}$$

The summation on the right hand side represents summation of an rithmetic-geometric sequence [42]. As $M \to \infty$ (based on sum of infinite rithmetic-geometric sequence with absolute value of common ratio of the geometric part of the sequence bounded by 1, i.e., $|e^{-\mu}| < 1$)

$$\lim_{M\to\infty} 2A\sum_{k=0}^{M}\frac{k}{M+1}e^{-\mu k} = \lim_{M\to\infty} 2A\frac{1}{M+1}\frac{e^{-\mu}}{(1-e^{-\mu})^2} = 0 \tag{67}$$

which implies that

$$\lim_{M\to\infty}\sum_{k=-M}^{M}\frac{|k|}{M+1}e_{ff,k}^2 \le \lim_{M\to\infty} A\sum_{k=-M}^{M}\frac{|k|}{M+1}e^{-\mu|k|} = 0 \tag{68}$$

The implication is that (based on Eqs. (63) and (68))

$$J_e = \frac{\left\|\mathbf{E}_{ff}\right\|_F}{\sqrt{M+1}} \to \left\|E_{ff}(q)\right\|_2 \quad \text{as} \quad M\to\infty \tag{69}$$

Figure Captions List

Fig. 1 Block diagram for feedforward tracking control

Fig. 2 Effect of basis functions (DCT, BPF and B-splines) on: (a) normalized RMS tracking error and (b) normalized RMS control input for various values of a (M = 1000, n = 990). The methods are also simulated for MP region (shaded) but the system can also be inverted in this region.

Fig. 3 Effect of basis functions (DCT, BPF, B-splines and Optimal) on (a) J_e and (b) J_c for various values of a (M = 1000, n = 990)

Fig. 4 Effect of basis functions (DCT, BPF, B-splines and Optimal) on (a) normalized RMS tracking error and (b) normalized RMS control input for various values of a (M = 1000, n = 990)

Fig. 5 Biaxial stage with flexible fixture

Fig. 6 Block diagram of the FBF controller and experimental setup

Fig. 7 Measured and modeled frequency response functions of the X and Y axes of the biaxial stage

Fig. 8 Singular values of the LSRs of the X and Y dynamics

Fig. 9 Desired path

Fig. 10 Desired position trajectories along the X and Y axes

Fig. 11 X and Y control inputs (i.e., modified position command) signals and tracking errors for optimal basis functions and B-splines (M = 10000, n = 600)

Fig. 12 Effect of zero location on normalized RMS tracking error for FBF (DCT, BPF), ZPETC and TS (for more details see [25])

Fig. 13 Effect of zero location on Frobenius norm metric for FBF, ZPETC and TS (for more details see [25])

Table Captions List

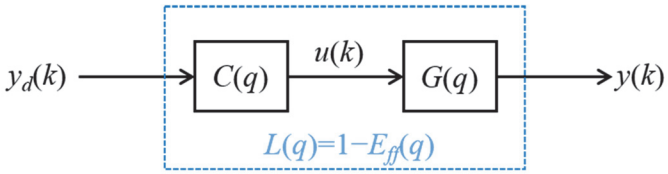

Fig. 1: Block diagram for feedforward tracking control

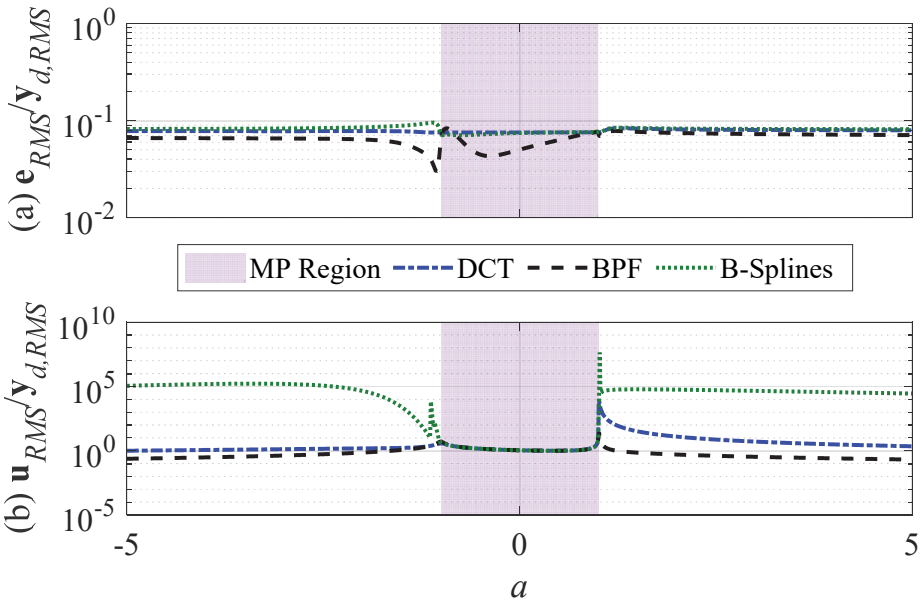

Fig. 2: Effect of basis functions (DCT, BPF and B-splines) on: (a) normalized RMS tracking error and (b) normalized RMS control input for various values of a (M = 1000, n = 990). The methods are also simulated for MP region (shaded) but the system can also be inverted in this region.

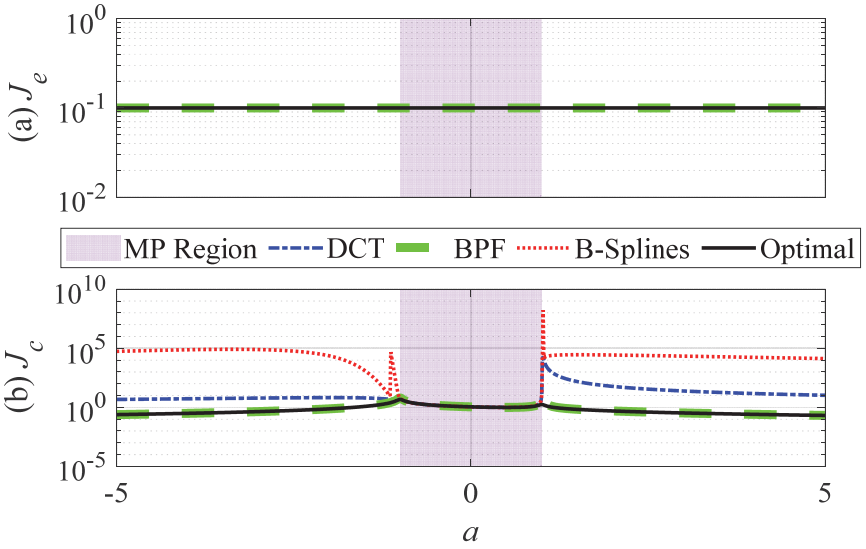

Fig. 3: Effect of basis functions (DCT, BPF, B-splines and Optimal) on (a) J_e and (b) J_c for various values of a (M = 1000, n = 990).

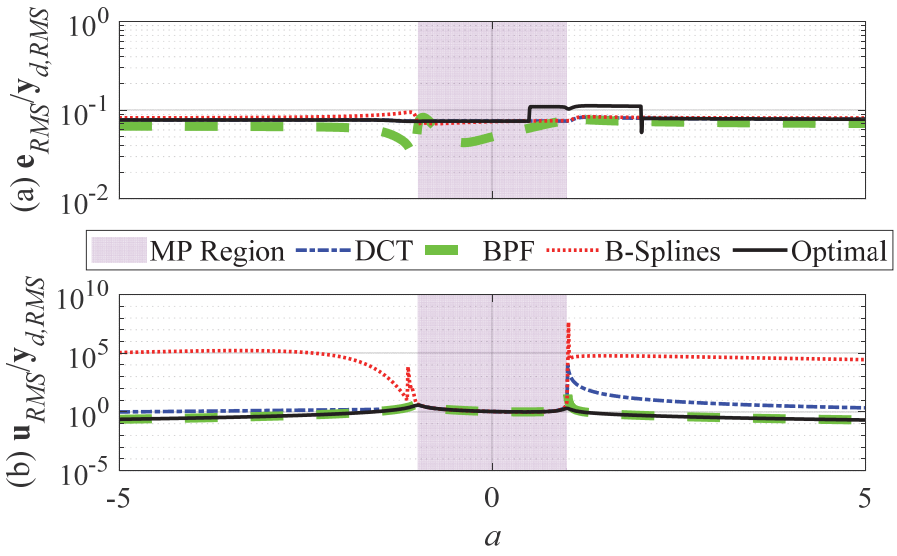

Fig. 4: Effect of basis functions (DCT, BPF, B-splines and Optimal) on (a) normalized RMS tracking error and (b) normalized RMS control input for various values of a (M = 1000, n = 990).

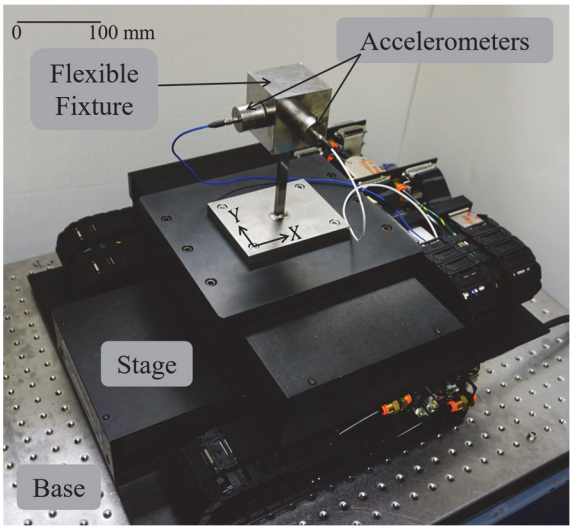

Fig. 5: Biaxial stage with flexible fixture

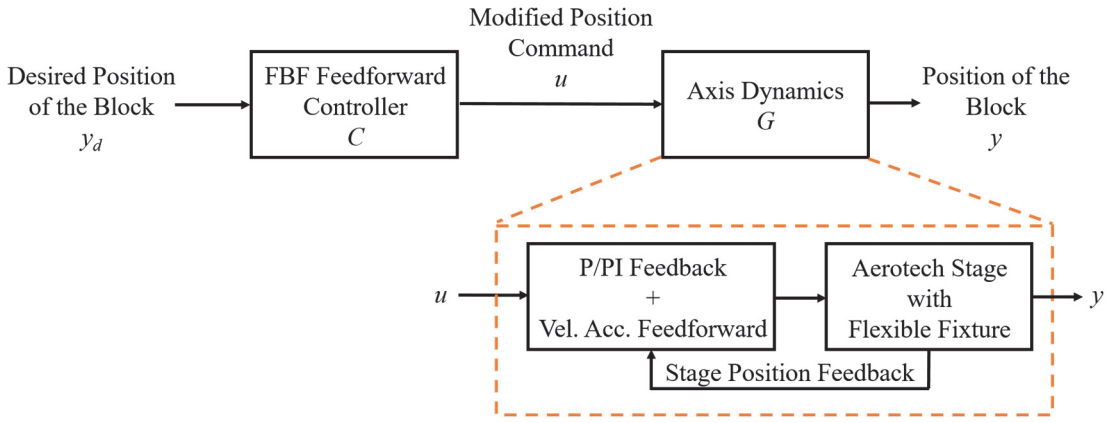

Fig. 6: Block diagram of the FBF controller and experimental setup

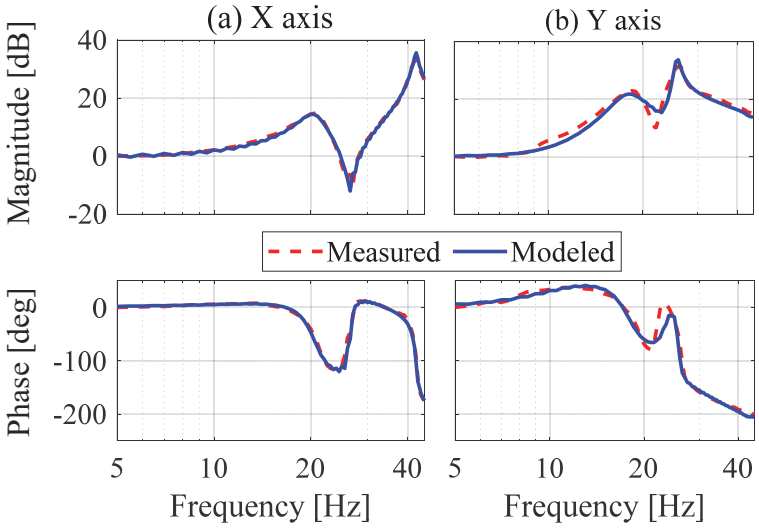

Fig. 7: Measured and modeled frequency response functions of the X and Y axes of the biaxial stage

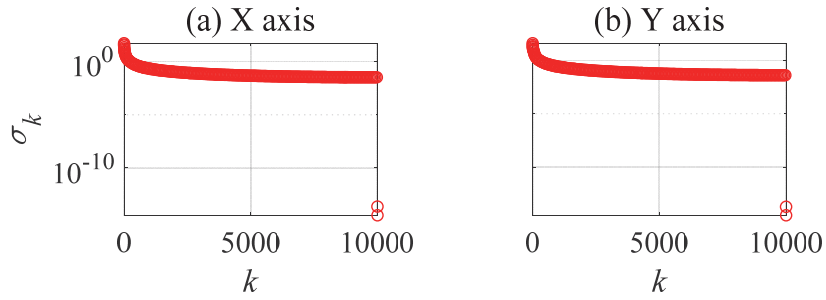

Fig. 8: Singular values of the LSRs of the X and Y dynamics

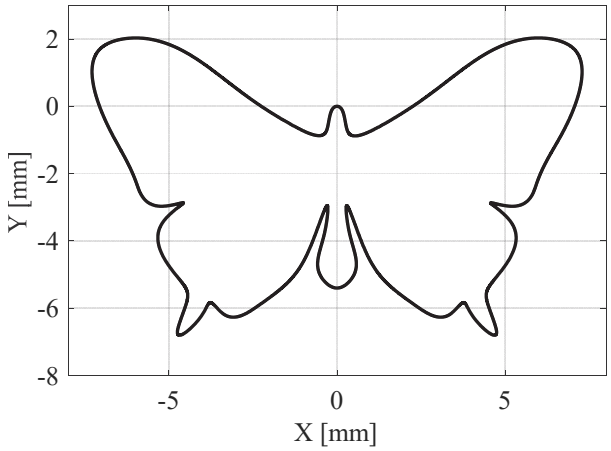

Fig. 9: Desired path

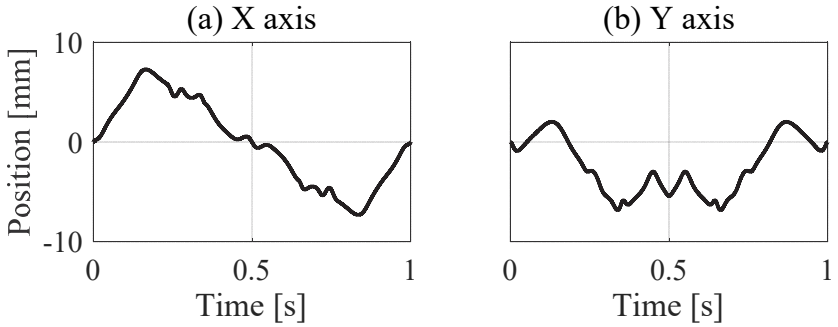

Fig. 10: Desired position trajectories along the X and Y axes

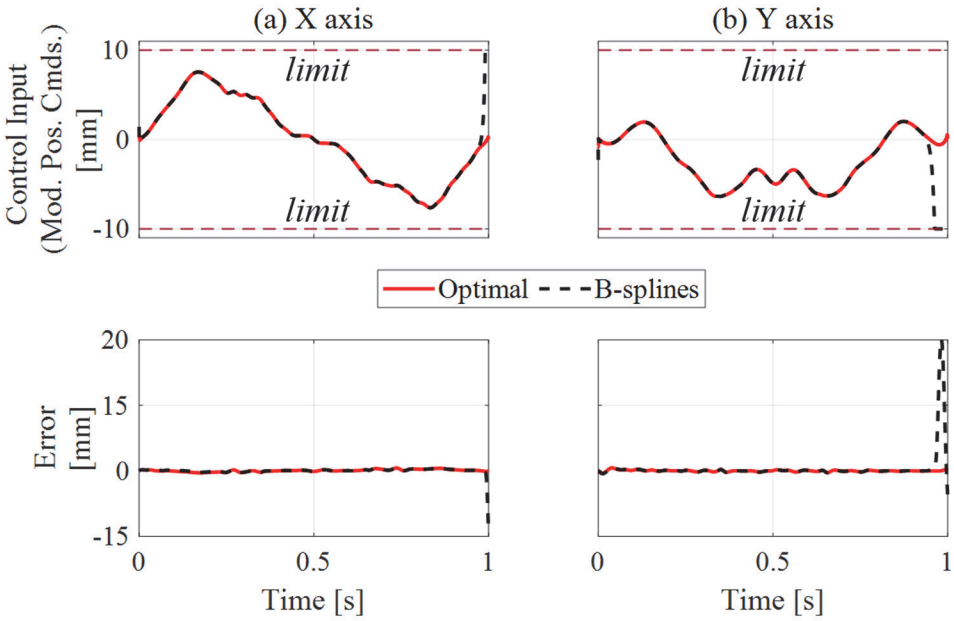

Fig. 11: X and Y control inputs (i.e., modified position command) signals and tracking errors for optimal basis functions and B-splines (M = 10000, n = 600)

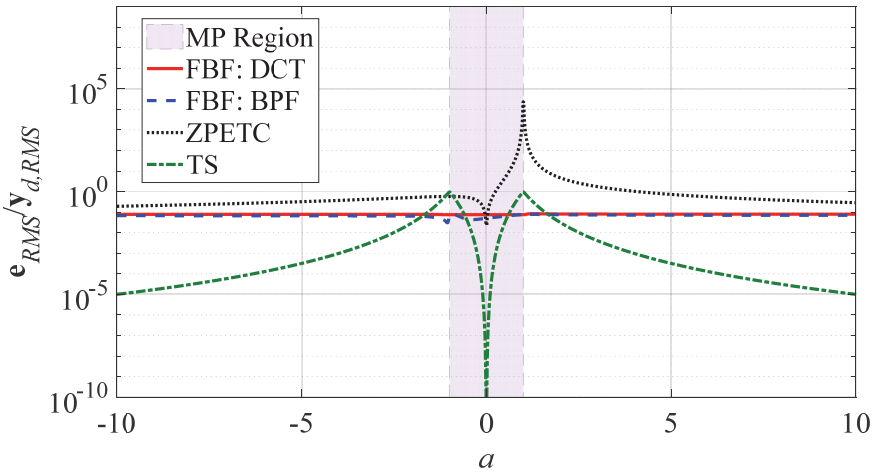

Fig. 12: Effect of zero location on normalized RMS tracking error for FBF (DCT, BPF), ZPETC and TS (for more details see [25])

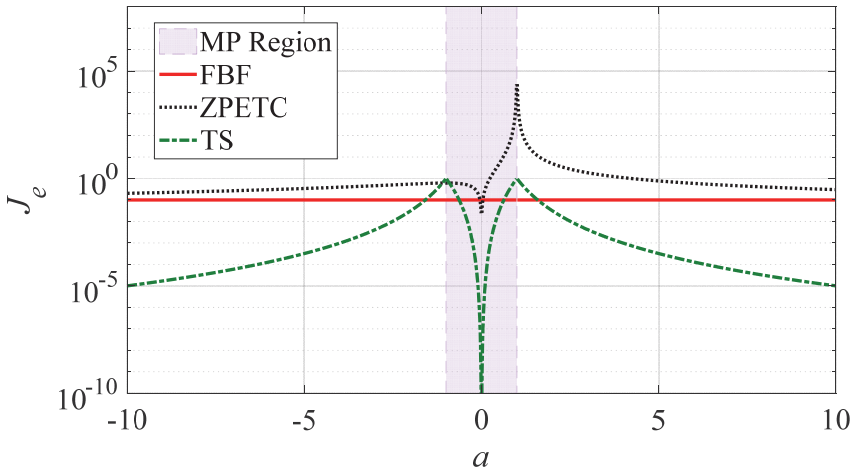

Fig. 13: Effect of zero location on Frobenius norm metric for FBF, ZPETC and TS (for more details see [25])

Tab. 1: Mean values of $\mathbf{e}_{RMS}/\mathbf{y}_{d,RMS}$ and $\mathbf{u}_{RMS}/\mathbf{y}_{d,RMS}$ over all a for different basis functions

Attribute	DCT	BPF	B-splines	Optimal
$\mathbf{e}_{RMS}/\mathbf{y}_{d,RMS}$	7.83×10^{-2}	6.62×10^{-2}	8.14×10^{-2}	8.28×10^{-2}
$\mathbf{u}_{RMS}/\mathbf{y}_{d,RMS}$	2.76×10^{1}	7.84×10^{-1}	1.02×10^{5}	7.06×10^{-1}

Tab. 2: Summary of tracking error and control effort for experiments

Basis Functions	X axis		Y axis	
	$\mathbf{e}_{RMS}/\mathbf{y}_{d,RMS}$	$\mathbf{u}_{RMS}/\mathbf{y}_{d,RMS}$	$\mathbf{e}_{RMS}/\mathbf{y}_{d,RMS}$	$\mathbf{u}_{RMS}/\mathbf{y}_{d,RMS}$
Optimal	0.06	1.05	0.05	0.98
B-Splines	0.17	1.08	0.94	1.12